

PHOTOCATALYTIC MEMBRANES FOR VIRUS INACTIVATION

By

Brian J. Starr

A THESIS

Submitted to
Michigan State University
in partial fulfillment of the requirements
for the degree of

Environmental Engineering – Master of Science

2015

ABSTRACT

PHOTOCATALYTIC MEMBRANES FOR VIRUS INACTIVATION

By

Brian J. Starr

Porous ceramic membranes are ideal candidates for use in environmental treatment and remediation. Ceramic membranes have a high chemical and thermal stability, allowing for aggressive cleaning and increased life span compared with polymeric membranes. For the same reasons, they are often used as substrates in photocatalytic membrane reactors. A multitude of techniques have been proposed to fabricate these photocatalytic membranes. In this study, Layer-by-layer self-assembly (LbL) and plasma enhanced chemical vapor deposition (PECVD) were used to create photocatalytic TiO₂ coatings on the support structure of ceramic disc microfiltration membranes. The resulting photocatalytic layers did not measurably reduce the membrane permeability. The LbL coated membrane degraded methylene blue at a higher rate compared to the PECVD coated membrane during UV filtration experiments. By assuming a plug flow reactor (PFR) model and normalizing the measured PFR rate constant by the catalytic efficiency of each catalyst, it is evident the LbL fabricated membrane benefited from the high catalytic efficiency of the Degussa P25 photocatalyst. Additionally, the LbL fabricated membrane's efficiency at inactivating MS2 and P22 bacteriophages was tested. While P22 was inactivated at a higher rate in batch reactors, MS2 was more susceptible to inactivation during UV dead-end filtration, with a maximum log removal value (LRV) of 4.9 achieved at the flow rate of 4×10^{-3} liters per minute for MS2 and only 1.6 LRV of P22 at the lower flow rate 3×10^{-3} liters per minute. With the coating on the permeate side of the membrane, this approach to virus inactivation is particularly promising in applications to waters with high degree of turbidity.

ACKNOWLEDGMENTS

Thanks to Craig Burck from The Department of Civil and Environmental Engineering at Michigan State University for his assistance in constructing the UV dead-end filtration cell. Becca Ives and Daniel Ginsburg from The Water Quality and Environmental Microbiology Laboratory at Michigan State University for their assistance with culturing bacteriophages. Ghada Jamal, Stephanie Roualdes, and Andre Ayrat at the European Institute of Membranes allowing use of their PECVD coating equipment and providing valuable guidance. My advisor, Volodymyr Tarabara, from The Department of Civil and Environmental Engineering at Michigan State University, for his continued support and direction throughout my graduate studies at Michigan State University.

TABLE OF CONTENTS

| | |
|--|-----|
| LIST OF TABLES | vi |
| LIST OF FIGURES | vii |
| CHAPTER 1 | 1 |
| 1.1 Introduction to titanium dioxide, photocatalytic reactions, and photocatalytic processes | 1 |
| 1.2 Ceramic Membranes | 4 |
| 1.3 Catalyst-membrane configuration..... | 8 |
| 1.4 Membrane-catalyst coating techniques..... | 11 |
| 1.5 Photocatalytic Membrane Applications | 13 |
| REFERENCES | 18 |
| CHAPTER 2 | 25 |
| 2.1 Introduction..... | 25 |
| 2.2 Approach..... | 28 |
| 2.2.1 Fabrication of photoactive membrane layer..... | 28 |
| 2.2.2 Important elements of photocatalytic membrane layers..... | 29 |
| 2.3 Experimental..... | 33 |
| 2.3.1 Reagents..... | 33 |
| 2.3.2 LbL assembly | 33 |
| 2.3.3 Plasma enhanced chemical vapor deposition | 35 |
| 2.3.4 Batch experiments..... | 36 |
| 2.3.5 Dead-end filtration experiments | 36 |
| 2.3.6 Measuring concentration of Methylene Blue | 39 |
| 2.3.7 UV fluence quantification..... | 39 |
| 2.3.8 Scanning electron microscope imaging..... | 40 |
| 2.4 Results and Discussion | 40 |
| 2.4.1 Titanium dioxide LbL assembly characterization | 41 |
| 2.4.2 Batch experiments on photocatalytic oxidation of methylene blue | 44 |
| 2.4.3 LbL and PECVD layer permeability..... | 46 |
| 2.4.4 UV MB dead-end filtration and analysis | 48 |
| 2.5 Conclusion | 53 |
| REFERENCES | 54 |
| CHAPTER 3 | 57 |
| 3.1 Introduction..... | 57 |
| 3.2 Experimental..... | 58 |
| 3.2.1 Reagents..... | 58 |
| 3.2.2 Batch Experiments | 58 |
| 3.2.3 Dead-end filtration experiments | 59 |
| 3.2.4 Quantification of bacteriophage concentration | 60 |
| 3.3 Results and Discussion | 61 |
| 3.3.1 Bacteriophage batch experiments | 61 |

3.3.2 UV Bacteriophage dead-end filtration 63
3.4 Conclusion 65
REFERENCES 66

LIST OF TABLES

| | |
|---|----|
| Table 1: Summary of UV induced titanium dioxide reactions [5]..... | 2 |
| Table 2: Summary of constants used in approach | 32 |
| Table 3: LbL and PECVD experimental parameters | 41 |
| Table 4: Experimental results of MB UV dead-end filtration experiments..... | 50 |
| Table 5: LbL self-assembly and PECVD coating quality..... | 51 |

LIST OF FIGURES

| | |
|--|----|
| Figure 1: Photocatalytic membrane configurations A) Selective layer coating B) Coupled photoactive-selective layer C) Support coating D) Embedded coating | 9 |
| Figure 2: Side view of an asymmetric ceramic membrane with a support photocatalytic layer of TiO ₂ | 27 |
| Figure 3: UV-microfiltration test apparatus. A: 1) Compressed air cylinder 2) Stainless steel feed tank 3) UV exposure box 4) Germicidal UV lamp 5) Membrane filtration cell with permeate UV window 6) Collection beaker with data acquisition system B: 1) UV exposure box 2) Germicidal UV lamp 3) Beaker and stir plate. | 38 |
| Figure 4: SEM images of LbL assembly of TiO ₂ nanoparticles on glass slides: A) (PAH+PSS)+TiO ₂ ; B) (PDADMAC+PAA) ₄ +TiO ₂ with catalyst in 0.01 M ionic strength solution; C) (PDADMAC+PAA) ₄ +TiO ₂ with PAA and TiO ₂ pH 2.5; D) (PDADMAC+PAA) ₄ +TiO ₂ with PAA and TiO ₂ pH 5; E) (PDADMAC+PAA) ₄ +TiO ₂ using high power probe sonicator; F) (PDADMAC+PAA) ₄ +TiO ₂ using bath sonicator..... | 43 |
| Figure 5: SEM images of (PDADMAC+PAA) ₄ +TiO ₂ coated ceramic membranes | 44 |
| Figure 6: MB batch experiments with A) 10 mg/L Degussa P25 catalyst B) 17 mg/L PECVD generated catalyst..... | 46 |
| Figure 7: Clean water flux tests with photocatalytic 0.14 μm membranes A) 5-layer LbL; B) 1-layer PECVD; C) 2-layer PECVD..... | 47 |
| Figure 8: MB UV dead-end filtration experiments A) 0.14 μm, 1 layer PECVD B) 0.14 μm 2 layers PECVD C) 0.14 μm, 5-layer LbL | 49 |
| Figure 9: Comparison of Photocatalytic Coatings A) Reactive flux B) $\Theta_{x,l_x}/\Theta_{y,l_y}$, where x is the coating used in the column and y is the PECVD coating with 2 layers..... | 52 |
| Figure 10: Bacteriophage batch testing using 1.25 mg/L Degussa P25 photocatalyst: A) MS2; B) P22 | 62 |
| Figure 11: UV dead-end filtration experiments A) MS2 B) P22..... | 64 |

CHAPTER 1

A review of titanium dioxide photocatalytic ceramic membranes

Titanium dioxide photocatalytic properties, related reactions, and photocatalytic treatment processes are reviewed in section 1.1. Section 1.2 highlights ceramic membrane fabrication techniques and research aimed at reducing costs of manufacturing membranes. Sections 1.3-1.5 discuss photocatalytic membrane processes, fabrication of photocatalytic membranes, and their application to water treatment.

1.1 Introduction to titanium dioxide, photocatalytic reactions, and photocatalytic processes

Titanium dioxide is a semiconducting metal capable of splitting water [1]. With irradiation from UV light, it has been widely shown to generate reactive oxygen species, including $\bullet\text{OH}$ and O_2^- [2-4]. The chain reactions necessary to generate these reactive species are summarized in Table 1 [5]. The reactions are initiated when UV light, with a wavelength less than 400 nm, excites electrons from the valence band (vb) to the conduction band (cb). This excitation leaves a reactive hole where the electron was previously located. The excited electron and reactive hole combine with bonded TiO_2 to migrate the reactive species to the crystal surface and delay recombination; these reactions are referred to as traps. In the presences of oxygen species, the trapped electron can combine with O_2 to create superoxide radicals and the reactive hole can combine with hydroxyl ions to create hydroxyl radicals. These species can then go on to create

other reactive oxygen species (ROS) or react with an organic contaminant. Additionally, the electron may return to the valence band and not result in a reaction.

Table 1: Summary of UV induced titanium dioxide reactions [5]

| Reaction | Description |
|---|--|
| $TiO_2 + UV \rightarrow e^- + hole^+$ | Electron excitation and hole creation |
| $e_{cb}^- \rightarrow e_{tr}^-$ & $hole_{vb} \rightarrow hole_{tr}$ | Electron and hole trapping |
| $e_{tr}^- + hole_{tr} \rightarrow e_{cb}^- + heat$ | Electron hole recombination |
| $O_2 + e_{tr}^- \rightarrow O_2^{*-}$ | Superoxide radical formation |
| $OH^- + hole_{tr} \rightarrow OH^*$ | Hydroxyl radical formation |
| $Organics + TiO_2 \rightarrow CO_2 + H_2O$ | Overall reaction of organic pollutant and TiO ₂ results in mineralization |

Significant research has been aimed at exploiting these pathways for the degradation of organic pollutants and inactivation of pathogens in water treatment [6-8]. Compared with chemical disinfection and oxidation, photocatalysis with TiO₂ produces significantly fewer disinfection byproducts (DBP) [9]. Additionally, TiO₂ has the ability to degrade DBP precursors that are present, resulting in fewer produced DBPs when TiO₂ disinfection is combined with chlorine [9].

Titanium dioxide generally exists in any of four phases; amorphous, brookite, anatase, and rutile, with anatase and rutile the most commonly generated crystallinity [10]. The crystallinity of TiO₂ can be altered by adjusting the catalyst preparation parameters, such as the sintering temperature [11]. As reviewed by Ismail and Bahnemann, anatase crystallinity is often the objective when generating TiO₂ photocatalyst, due to its high photoactivity [12]. This is not true for all

reactions, as Tay found brookite to be more productive in generating H₂ than anatase [10]. Interestingly, Bacsa and Kiwi showed that pure anatase was less photoactive than a mixture of rutile and anatase [13]. From their experimental work a ratio of 70% anatase to 30% rutile was more efficient than Degussa P25, a highly efficient TiO₂ catalyst. A similar result was obtained by Bakardjeiva et al, who found 100% anatase exhibited poorer photodegradation of 4-chlorophenol, while a mixture of ~77% anatase and 23% rutile enhanced degradation [14]. Lastly, the lower surface areas, due to elevated calcination temperatures, associated with rutile may account for its lower apparent catalytic efficiency [15]. A direct comparison on the inherent catalytic properties of rutile and anatase must account these physical changes, as well as differences in the crystal phase composition.

Degussa P25, is a commercially available TiO₂ nanoparticle often cited as a standard for high photoactivity [14]. It is frequently reported as a simple mixture of anatase and rutile crystallinity [16, 17]. Further investigation has shown that although the XRD graphs of P25 and simple mixtures of pure anatase and pure rutile are similar, images with TEM show that P25 contains complicated amorphous/anatase and amorphous/rutile regions, that are not present in the simple mixtures [18]. The high photoactivity of P25 has been attributed to these complicated multi-crystalline regions. More recently, this finding was contradicted by Ohtani [19], who found the phases did not interact and suggests there is no evidence of a synergism between the mixed phases.

Metal doping of titanium dioxide is an active area of research in photocatalysis. Various benefits have been seen, such as improved bacterial disinfection with Ag-TiO₂ membranes [20] and increased visible light photoactivity with nickel [21]. Experiments testing a multitude of M-TiO₂ coatings under visible light have demonstrated that improved reaction kinetics are often pollutant

specific [22]. Interestingly, metal doping TiO_2 has been shown to change the anatase-rutile phase conversion temperature. Specifically, ruthenium inhibited the conversion from anatase to rutile up to 700°C [22]. This can become important in photocatalytic membrane fabrication techniques that require high sintering temperatures, such as hollow fiber fabrication.

Photocatalytic processes using TiO_2 are generally implemented by either suspending the TiO_2 in a photoreactor or immobilizing it on the surface of a contactor [23]. Suspended reactors have the benefit of higher TiO_2 loading, but require an additional process unit for photocatalyst recovery [24]. Immobilized TiO_2 reactors have lower catalyst loadings, but do not require catalyst recovery [24].

Immobilized photocatalytic processes require a contactor. Contactors can take various geometries, such as the smooth surface of a reaction vessel [26] or porous particles [27]. Properties of contactors include high surface area, chemical and thermal stability, and ease of cleaning. With the addition of a separation layer, a porous contactor may also serve as a membrane. Depending on where the catalyst is deposited, the use of a membrane as a contactor provides several benefits to both the membrane and the photocatalytic processes, including contaminant concentration on the catalyst, reduced turbidity for the improved efficiency of UV light, and reduced membrane fouling. Due to their mechanical and chemical stability, ceramic membranes are the most frequently used membrane contactors.

1.2 Ceramic Membranes

Inorganic membranes are available in a wide variety of materials, geometries, and configurations. Due to their chemical and thermal stability, inorganic membranes are often used

in processes with demanding conditions that justify their additional cost compared to polymeric membranes. Inorganic membranes can be made of oxide, metal, carbon, or other materials [28]. Commonly available geometries include disk and tubular [29]. Multi-channel tubular membranes, referred to as monoliths, are commercially available and provide an increased surface area density [29]. Inorganic membranes can be porous or dense. The pore size cutoff between porous and dense is not precisely defined, but dense inorganic membranes are used in gas phase separation processes, whereas porous inorganics are used in water treatment. This review will focus on porous ceramic membranes, which are suitable for use as photocatalytic contactors and in water treatment processes.

Porous ceramic membranes are typically asymmetrical and can be defined by several layers. The active layer has the smallest pore size and performs the separative process. This layer is typically made very thin to reduce its hydraulic resistance. The outer layers have increasingly larger pore sizes and act to support the thin active layer. Slip casting, tape casting, pressing, and extrusion are all methods used to fabricate support structures [30]. The active layer is typically formed via advanced techniques, such as sol-gel precipitation, chemical vapor deposition, or dip coating [30].

In slip casting, tape casting, and pressing methods a pliable paste of ceramic particles is formed into a solid structure by removing solvent from the paste. This structure is then dried and sintered to create a stable support. During slip casting, the ceramic paste is applied to a porous mold and capillary forces remove the solvent. The tape casting process uses a casting knife to deposit a film of suspended ceramic and the solvent is removed by evaporation. Pressing techniques use force to remove the solvent. Extrusion methods force a plastic-like paste through a nozzle to give it shape. When force is not being applied, the paste has increased rigidity.

When forming the active layer using sol-gel processes, a solution of ceramic precursor is applied to a support structure and ceramic is then precipitated on the surface. This process has higher control of pore size, porosity, and film thickness than the casting and pressing methods. With dip coating, a substrate is submersed in a suspension of ceramic particles. The layers morphology can be adjusted by varying the suspension viscosity, contact time, and dipping speed. Chemical vapor deposition uses a carrier gas to bring a flux of precursor to a substrates surface. A reaction then occurs either in the gas phase or on the substrate itself, resulting in a thin film of deposited ceramic.

Active research in ceramic membrane fabrication focuses on improving the stability of the membranes [31-32], separative functionality [33-34], and/or reducing manufacturing costs [35-36]. While stability is a critical property in processes such as high temperature flue gas treatment, membranes in water treatment are not typically exposed to such extreme conditions. Research on improving ceramic membrane separative functionality centers on dense membrane fabrication, often for gas separation. In water treatment, which uses porous membranes, important research to allow widespread application is centered on reducing manufacturing cost. Major costs associated with ceramic membrane fabrication are expensive precursor materials such as alumina, zirconia, titania, and silica and the energy intensive sintering process [37]. Sintering is an additional cost that polymeric membrane fabrication does not require. Lower cost materials, such as clay, sawdust, fly ash, calcium carbonate, and quartz have all been successfully used in creating ceramic membranes. New low cost ceramic membrane fabrication techniques blend a selection of these precursors in order to create a stable porous membrane. Clay is used for its low plasticity and high refractory properties [38]. Calcium carbonate is often used as a pore former [39]. Quartz or similar materials add strength to the membrane [38]. Fly

ash is a readily available byproduct of the coal industry and serves as a filler material.

Membranes utilizing fly ash require binders, such as polyvinyl alcohol [40].

In effort to make ceramic technologies more affordable, recent research has shown ceramic membranes can be fabricated using locally available natural materials. Belibi et al. fabricated a microfiltration membrane using only Cameroonian clay, with sawdust as a pore former [40].

Wang et al. developed microfiltration membranes using a mix of Portland cement and quartz, which did not require any sintering [42].

Membranes fabricated with low cost materials are typically prepared by uniaxial wet or dry compaction or the paste methodology. In the paste method, the precursors are simply mixed with a small amount of water, placed in a mold, slowly dried, and then sintered [37]. In the compaction method, similar to conventional ceramic membrane support fabrication, the precursors are homogenously mixed with or without water, pressed with mechanical force, and sintered [39]. A comparison between the two methods showed that uniaxial compaction resulted in larger pore sizes compared with the paste method, even with the same precursor formulation [39]. Vasanth et al. has shown these fabrication techniques can produce a ceramic membrane for approximately \$61 per square meter compared to \$500 per square meter for a similar ceramic alumina membrane.

Low cost ceramics have been successfully applied in bacterial separation [36], oil-water separation [39], and food processing [43]. Further testing is needed to understand the chemical and thermal stability of these low cost membranes. Only one of the above cited studies investigated the mechanical strength and hydraulic stability [41], but as Buekenhoud [44] reviewed, dynamic tests with corrosive fluids are needed to understand the true chemical stability of these membranes.

1.3 Catalyst-membrane configuration

Photocatalytic membranes can be categorized into three groups based on the catalyst location; membranes with selective layer coating, membranes with support coating, or embedded reactors. Locating the photocatalyst on the selective layer is the most commonly reported configuration. With this configuration (Figure 1A), there are several synergistic benefits to both the membrane and photocatalytic process. During filtration, the pollutant is concentrated on the catalyst due to the concentration polarization effect, resulting in faster reaction kinetics. The catalyst reaction may also benefit the membrane separation process by degrading pollutants that cause fouling [45]. Additionally, since titanium dioxide is hydrophilic, TiO_2 coated selective layers have shown increased water flux compared to uncoated membranes [46].

In order to reduce the hydraulic resistance of the coated membrane, research has been performed into creating a dual-purpose selective and photoactive layer of TiO_2 , referred to as coupled functionality. With these membranes, the catalyst layer acts as the mechanical barrier to pollutants and is also the photoactive layer (Figure 1B). This eliminates the need for a separate catalyst layer and selective layer. The primary drawback of coupled membranes is that the separative functionality and photoactivity may have distinctly different optimized requirements. For example, a 3 nm coupled TiO_2 membrane produced by Wu et al. [11] had a molecular weight cut off of 4,000 kDa, while they reported a commercially available non-photoactive membrane with the same pore size made of silica/zirconia had a MWCO of just 1,000 kDa. This difference was attributed to the more favorable interaction between the non-photoactive membrane material and contaminants.

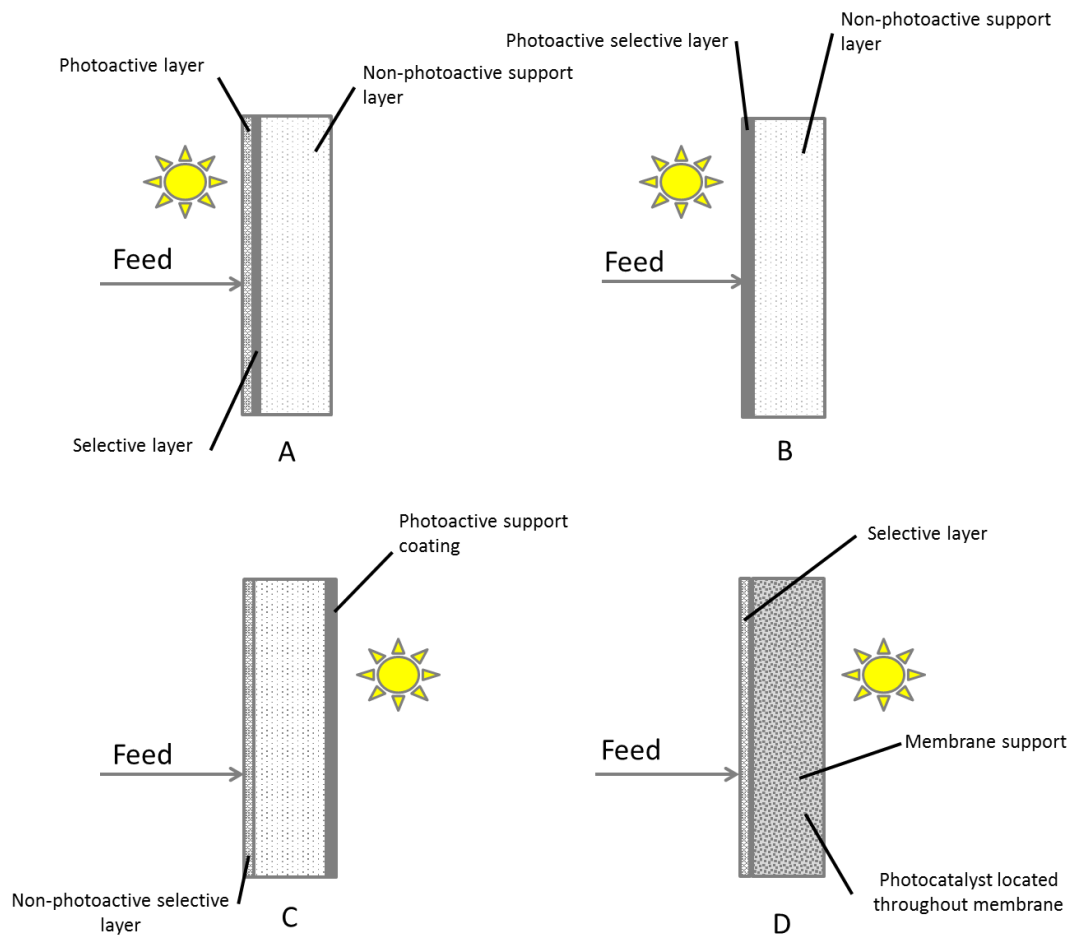


Figure 1: Photocatalytic membrane configurations A) Selective layer coating B) Coupled photoactive-selective layer C) Support coating D) Embedded coating

Coating the membrane support (Figure 1C), has the benefit of allowing optimization of the selective layer and photoactive layers independently. This process arrangement was first proposed by Bosc et al. [47], though experimental results were not reported. Having the photoactive layer on the outside of the membrane also allows for a simpler arrangement of coupling between the source of UV irradiation and the photocatalytic surface, especially when ceramic tubular membranes are employed. Also, the membrane will remove turbidity prior to photocatalysis, improving catalytic performance through two mechanisms. First, the less turbid water will allow for higher fluence on the catalyst. Second, the turbidity causing particles react with reactive oxygen species, reducing the ROS concentration available for disinfection. Literature on membrane support side coatings is limited. In one study [48], both the feed and permeate side of a ceramic support were coated; the authors showed that both layers of TiO_2 contributed to the degradation of a model pollutant.

The embedded reactor has catalyst coated or embedded throughout the matrix of the membrane (Figure 1D.) In contrast to the previous configurations, catalyst is not limited to outer layers on the feed or support side. Catalytic membrane reactors with this configuration are the most commonly developed due to the increased pollutant-catalyst contact time. Since photocatalytic reactions require catalyst exposure to UV light, photocatalytic membranes with this configuration have seen limited development. An exception are photocatalytic membranes that use photoactive catalyst as the only membrane material. Zhang et al. [16] created photocatalytic hollow fibers through membrane spinning and phase inversion that resulted in pure TiO_2 hollow fibers. Due to their small size, hollow fibers have a high specific surface area, which is beneficial to photocatalytic reactions and membrane separation. A significant limitation of this technique is that photoactivity decreases with increasing sintering temperature while high

sintering temperatures are needed to give mechanical strength to the hollow fibers. In permeability experiments the authors used hollow fiber membranes prepared with low photoactivity due to the weak mechanical strength of the hollow fibers with high photoactivity. Similar to the dual-functionality membranes, the photoactive and membrane separation function need to optimize simultaneously, which may be a challenge.

1.4 Membrane-catalyst coating techniques

Methods of fabrication of photocatalytic membranes can be divided broadly into two groups of techniques: 1) deposition of existing (pre-formed) nanoparticles on the membrane and 2) the use of TiO₂ precursors to precipitate photocatalyst on the membrane. When using existing nanoparticles, they are typically suspended in solution and the substrate is coated using a dip coating procedure [49-50]. This has the benefit of simple assembly techniques and the known high photoactivity of the particle, such as Degussa P25 [51]. The drawback is that the particles may not be optimally placed on the membrane, resulting in a significant reduction in flux [52]. In dip coating, high concentrations of particles are suspended, often with the aid of a dispersant [49]. A substrate is then dipped in the catalyst suspension and withdrawn at a constant rate. The deposited film thickness is dependent on withdrawal speed, suspension viscosity, evaporation rate, and substrate width [53].

Similar to dip coating, LbL self-assembly is a simple method that has been used to create thin films from existing nanoparticles. In LbL self-assembly, polyelectrolytes are coated on a substrate, resulting in a modification of the surface charge characteristics. The polyelectrolyte coated substrate is then submersed in a low concentration nanoparticle suspension.

Nanoparticles adhere to the polyelectrolytes via electrostatic interactions. LbL self-assembly can be completed by either two-step or three-step assembly. In three-step assembly, a substrate is coated with multiple bilayers of alternatively charged polyelectrolytes [54]. The terminating layer has the same charge as the substrate. The oppositely charged nanoparticles are then adhered to this layer. In two-step assembly, a single polyelectrolyte is used [55]. LbL self-assembly has been applied to non-photoactive catalytic membrane reactors. Dotzauer utilized LbL self-assembly to create a catalytic wall reactor membrane with a sub-monolayer deposition of gold particles on a polymeric membrane [56]. A review of literature could not find examples of LbL self-assembly used in TiO₂ photocatalytic membrane fabrication.

Using TiO₂ precursors, TiO₂ crystals have been formed in place on various membrane materials, with the aim of improving flux, selectivity, photoactivity, or all of the above. Sol-gel dip coating is a common technique that utilizes TiO₂ precursors. Typically, a precursor, such as titanium tetraisopropoxide (TTIP), is added to a solution containing surfactants and other reagents that cause the TTIP to hydrolyze and form TiO₂ [57]. The membrane is dipped into the sol, dried, and then sintered. The surfactants structure the precursors. These organics are removed through sintering, leaving an organized TiO₂ structure.

Varying the surfactants and adding copolymers can create unique crystal structures, such as cylindrical or hexagonal pores [47]. This technique is most beneficial for coupled selective and photoactive coatings, allowing the pore size to be tuned by varying assembly conditions. Additionally, varying the drying, stabilizing, and sintering temperature and duration can also lead to structural changes [47]. The sol-gel dip coating procedure can be repeated, adjusting the parameters to create a hierarchical structure with improve permeability compared to non-hierarchical multilayers, while preserving photoactivity [58]. Non-selective nanostructures, such

as nano-ribbons and nano-wires, have been generated from TTIP precursors by controlling the hydrolysis rate [52]. The authors found these coated membranes to have a significantly higher permeability, while maintaining a similar photoactivity to a P25 coated membrane.

Chemical vapor deposition (CVD) has been used to deposit TiO₂ films onto various porous substrates, including alumina, activated carbon, and silica [27]. This technique has been extended to produce photoactive TiO₂ membranes [48]. Stated benefits of CVD are scalability, reduced manufacturer costs, and improved permeability. Though comprehensive comparisons on these metrics for dip coating, LbL self-assembly, sol-gel dip coating and CVD could not be found in literature. One comparison study on the photoactivity found that both CVD and sol-gel dip coating could produce equally high photoactivity [59]. A drawback of CVD is the high temperature required during the deposition. The previously cited study uses temperatures up to 600°C during deposition. With the aid of plasma, the reactor temperature can be lowered to near room temperature [60]. Plasma enhanced vapor deposition excites the TiO₂ precursor in the vapor phase into a plasma using R.F., causing the photocatalyst to then form on the substrate. This reduces energy demand of the process and allows for coating on temperature sensitive materials.

1.5 Photocatalytic Membrane Applications

Titanium dioxide photocatalytic membranes have many potential applications in water treatment, including: mineralization of organic pollutants, improved membrane flux, and inactivation of pathogens. There have been several proposed mechanisms for the increased flux of TiO₂ coated membranes, including increased hydrophilicity, reduced biofilm generation, and degradation of

fouling contaminants. Bae et al. [46] incorporated P25 photocatalyst into the matrix of a membrane to create an embedded photocatalytic membrane and used phase inversion to create an asymmetric membrane. In crossflow filtration of activated sludge, this membrane showed a reduction in fouling compared with a neat membrane. The reduced fouling was attributed solely to the hydrophilicity of the nanoparticles, as the membranes were not illuminated with UV. The authors also found that a deposition of catalyst on the selective layer reduced fouling further than membranes with catalyst embedded in the membrane matrix. For photocatalytic membranes, this leads to a synergy, as photocatalytic membrane configurations typically have TiO₂ coating externally. The increased hydrophilicity of TiO₂ coated membranes was confirmed with water contact angle measurements on Al₂O₃ membranes that had a thin layer of TiO₂ deposited on the surface of a membrane and within the pore channels [61]. This membrane also exhibited an initial flux increase of 30-40% prior to any fouling compared to the membrane without coating. This flux increase was maintained throughout fouling experiments using stable oil-water emulsions.

Bio-fouling can lead to increased operational costs through higher transmembrane pressure requirements and increased cleaning frequency [62]. Titanium dioxide coatings reduce biofilm formation by increasing hydrophilicity of the membrane, as discussed earlier, and due to their photocatalytic reactivity [63]. Ciston et al. delineated the hydrophilic and photocatalytic contributions by comparing photoactive anatase membranes to non-photoactive rutile TiO₂ coatings. The results indicate that the hydrophilic effects are important in preventing the early adhesion of bacteria to the membrane and photocatalysis prevents long term growth of established films. The reduction in fouling attributable to photoactivity is only applicable for

membranes with selective layer catalyst coatings, whereas membranes with only permeate side surface coatings will not benefit from reduced fouling.

Both suspended and immobilized titanium dioxide has been investigated for application in mineralizing organic pollutants [26]. As compared to traditional membrane processes, photocatalytic treatment of organic pollutants mineralizes the pollutant, rather than concentrating it. Photocatalytic membranes have been studied in this application, most commonly using dyes as a model [49, 16]. One drawback photocatalytic membranes have is the limited contact time as compared to suspended TiO₂ reactors. Wang et al. found the maximum one pass decomposition of Acid Red 4 dye to be about 65% for dead-end filtration, but this decreases rapidly with increasing flowrate [49]. Similarly, Zhang et al. demonstrated an 82% removal of Direct Black 168 with TiO₂ photocatalytic membrane, though this required an extended run time of 300 minutes [16]. For treatment of highly concentrated dyes, coating the membrane permeate side may provide improved reaction kinetics from the increased UV fluence, due to reduced dye concentration by the membrane. In addition to dyes, other organic pollutants have been tested. Kovaleva et al have studied the removal of benzothiazoles [64], Molinari et al tested the degradation of 4-nitrophenol with the use of polymeric photocatalytic membranes [65], and Zhang removed sodium dodecylbenzene sulfonate with composite ceramic nano-rod membranes [66].

Pharmaceutical and personal care products (PPCPs), such as 4-Methylbenzylidene Camphor and Octocrylene, have been found to persist through conventional wastewater treatment processes and be discharged to the environment [67]. Titanium dioxide photocatalytic membranes have been shown to degrade a number of PPCPs, including norfluxentine, atrazine, and trimethoprim [68], but suffer from a shortcoming of other treatment options for PPCPs [69], in that the

reaction rate is very dependent on the particular pollutant [70]. Pharmaceuticals and personal care products are typically present in minute concentrations and may benefit from active layer coating configurations, taking advantage of concentration polarization, though data on this potential synergism for PPCP removal has not been published.

Disinfection with UV photocatalysis has obvious benefits due to the generation of reactive oxygen species that have been shown to inactivate a wide spectrum of pathogens, including bacteria, fungi, algae, protozoa, viruses, and bacterial toxins [71, 4]. Compared to UV-only inactivation, photocatalyst can reduce the time required to achieve a 4-log reduction of *E. coli* by half [57]. The vast majority of research into photocatalytic disinfection, as extensively summarized by Foster [4], has been with suspended TiO₂ or thin films, not membranes. But as pointed out by Rincón [72], turbidity reduces photocatalytic disinfection by scattering light, aggregating suspended photocatalyst, and reducing the concentration of reactive oxygen species. Immobilizing titanium dioxide on the permeate side of the membrane could mitigate these turbidity related issues.

While titanium dioxide membrane coatings have shown promising results for water treatment, the application of these coatings as a viable water treatment technology outside of a laboratory requires additional research. Most studies have focused on the photoactivity, antifouling, and permeability of these membranes, but only one of the articles reviewed here looked at the durability of the coatings over wash cycles [20]. Durability becomes critical when separation and photocatalysis are coupled into one layer and act as the sole barrier, especially when removing pathogenic microorganisms. Furthermore, to replace existing technology, the TiO₂ membranes will need to be more cost efficient than current processes. Only one study [48] compared the energy requirement of photoactive membrane processes to membrane only

separation and interestingly found photoactive membranes have the potential to reduce energy demand. Lastly, combining the low cost ceramic membrane manufacturing techniques reviewed earlier with the latest research into titanium dioxide photocatalysis may yield a photocatalytic membrane suitable for widespread adoption.

REFERENCES

REFERENCES

1. Fujishima, A.; Honda, K., Electrochemical Photolysis of Water At a Semiconductor Electrode. *Nature* 1972, 238 (5358), 37-38.
2. Kikuchi, Y.; Sunada, K.; Iyoda, T.; Hashimoto, K.; Fujishima, A., Photocatalytic bactericidal effect of TiO₂ thin films: Dynamic view of the active oxygen species responsible for the effect. *Journal of Photochemistry and Photobiology a-Chemistry* 1997, 106 (1-3), 51-56.
3. Chang, C. Y.; Hsieh, Y. H.; Hsieh, L. L.; Yao, K. S.; Cheng, T. C., Establishment of activity indicator of TiO₂ photocatalytic reaction-Hydroxyl radical trapping method. *Journal of Hazardous Materials* 2009, 166 (2-3), 897-903.
4. Foster, H. A.; Ditta, I. B.; Varghese, S.; Steele, A., Photocatalytic disinfection using titanium dioxide: spectrum and mechanism of antimicrobial activity. *Applied Microbiology and Biotechnology* 2011, 90 (6), 1847-1868.
5. Chong, M. N.; Jin, B.; Chow, C. W. K.; Saint, C., Recent developments in photocatalytic water treatment technology: A review. *Water Research* 2010, 44 (10), 2997-3027.
6. Teoh, W. Y.; Denny, F.; Amal, R.; Friedmann, D.; Madler, L.; Pratsinis, S. E., Photocatalytic mineralisation of organic compounds: a comparison of flame-made TiO₂ catalysts. *Topics in Catalysis* 2007, 44 (4), 489-497.
7. Cho, M.; Chung, H. M.; Choi, W. Y.; Yoon, J. Y., Different inactivation Behaviors of MS-2 phage and *Escherichia coli* in TiO₂ photocatalytic disinfection. *Applied and Environmental Microbiology* 2005, 71 (1), 270-275.
8. Triantis, T. M.; Fotiou, T.; Kaloudis, T.; Kontos, A. G.; Falaras, P.; Dionysiou, D. D.; Pelaez, M.; Hiskia, A., Photocatalytic degradation and mineralization of microcystin-LR under UV-A, solar and visible light using nanostructured nitrogen doped TiO₂. *Journal of Hazardous Materials* 2012, 211, 196-202.
9. Richardson, S. D.; Thruston, A. D.; Collette, T. W.; Patterson, K. S.; Lykins, B. W.; Ireland, J. C., Identification of TiO₂/UV disinfection byproducts in drinking water. *Environmental Science & Technology* 1996, 30 (11), 3327-3334.
10. Tay, Q. L.; Liu, X. F.; Tang, Y. X.; Jiang, Z. L.; Sum, T. C.; Chen, Z., Enhanced Photocatalytic Hydrogen Production with Synergistic Two-Phase Anatase/Brookite TiO₂ Nanostructures. *Journal of Physical Chemistry C* 2013, 117 (29), 14973-14982.
11. Wu, L. Q.; Huang, P.; Xu, N. P.; Shi, J., Effects of sol properties and calcination on the performance of titania tubular membranes. *Journal of Membrane Science* 2000, 173 (2), 263-273.

12. Ismail, A. A.; Bahnemann, D. W., Mesoporous titania photocatalysts: preparation, characterization and reaction mechanisms. *Journal of Materials Chemistry* 2011, 21 (32), 11686-11707.
13. Bacsa, R. R.; Kiwi, J., Effect of rutile phase on the photocatalytic properties of nanocrystalline titania during the degradation of p-coumaric acid. *Applied Catalysis B-Environmental* 1998, 16 (1), 19-29.
14. Bakardjieva, S.; Subrt, J.; Stengl, V.; Dianez, M. J.; Sayagues, M. J., Photoactivity of anatase-rutile TiO₂ nanocrystalline mixtures obtained by heat treatment of homogeneously precipitated anatase. *Applied Catalysis B-Environmental* 2005, 58 (3-4), 193-202.
15. Silva, Cláudia Gomes, and Joaquim Luís Faria., Anatase Vs. Rutile Efficiency on the Photocatalytic Degradation of Clofibrac Acid Under Near UV to Visible Irradiation. *Photochemical & photobiological sciences: Official journal of the European Photochemistry Association and the European Society for Photobiology* 8.5 (2009): 705.
16. Zhang, X. W.; Wang, D. K.; Lopez, D. R. S.; da Costa, J. C. D., Fabrication of nanostructured TiO₂ hollow fiber photocatalytic membrane and application for wastewater treatment. *Chemical Engineering Journal* 2014, 236, 314-322.
17. Porter, J. F.; Li, Y. G.; Chan, C. K., The effect of calcination on the microstructural characteristics and photoreactivity of Degussa P-25 TiO₂. *Journal of Materials Science* 1999, 34 (7), 1523-1531.
18. Bickley, R. I.; Gonzalezcarreno, T.; Lees, J. S.; Palmisano, L.; Tilley, R. J. D., A structural investigation of titanium-dioxide photocatalysts. *Journal of Solid State Chemistry* 1991, 92 (1), 178-190.
19. Ohtani, B.; Prieto-Mahaney, O. O.; Li, D.; Abe, R., What is Degussa (Evonik) P25? Crystalline composition analysis, reconstruction from isolated pure particles and photocatalytic activity test. *Journal of Photochemistry and Photobiology a-Chemistry* 2010, 216 (2-3), 179-182.
20. Liu, L.; Liu, Z. Y.; Bai, H. W.; Sun, D. D., Concurrent filtration and solar photocatalytic disinfection/degradation using high-performance Ag/TiO₂ nanofiber membrane. *Water Research* 2012, 46 (4), 1101-1112.
21. Kim, D. H.; Choi, D. K.; Kim, S. J.; Lee, K. S., The effect of phase type on photocatalytic activity in transition metal doped TiO₂ nanoparticles. *Catalysis Communications* 2008, 9 (5), 654-657.
22. Choi, J.; Park, H.; Hoffmann, M. R., Effects of Single Metal-Ion Doping on the Visible-Light Photoreactivity of TiO₂. *Journal of Physical Chemistry C* 2010, 114 (2), 783-792.
23. Chong, M. N.; Jin, B.; Chow, C. W. K.; Saint, C., Recent developments in photocatalytic water treatment technology: A review. *Water Research* 2010, 44 (10), 2997-3027.

24. Shan, A. Y.; Ghazi, T. I. M.; Rashid, S. A., Immobilisation of titanium dioxide onto supporting materials in heterogeneous photocatalysis: A review. *Applied Catalysis a-General* 2010, 389 (1-2), 1-8.
25. Mahmoodi, N. M.; Arami, M., Bulk phase degradation of Acid Red 14 by nanophotocatalysis using immobilized titanium(IV) oxide nanoparticles. *Journal of Photochemistry and Photobiology a-Chemistry* 2006, 182 (1), 60-66.
26. Brezova, V.; Jankovicova, M.; Soldan, M.; Blazkova, A.; Rehakova, M.; Surina, I.; Ceppan, M.; Havlinova, B., Photocatalytic Degradation of p-Toluenesulphonic Acid in Aqueous Systems Containing Powdered and Immobilized Titanium-Dioxide. *Journal of Photochemistry and Photobiology a-Chemistry* 1994, 83 (1), 69-75.
27. Ding, Z.; Hu, X. J.; Yue, P. L.; Lu, G. Q.; Greenfield, P. F., Synthesis of anatase TiO₂ supported on porous solids by chemical vapor deposition. *Catalysis Today* 2001, 68 (1-3), 173-182.
28. Vrijen Hoek, E. M.; Tarabara, V. V., *Encyclopedia of membrane science and technology*. Wiley, Hoboken, New Jersey, 2013; pp. 3 volumes (xviii, 2347 pages).
29. "Ceramic Membranes for Crossflow Filtration - TAMI Industries - Advanced Ceramic Filtration." TAMI Industries. N.p., n.d. Web. 2015. <<http://www.tami-industries.com/>>.
30. Li, K., *Ceramic membranes for separation and reaction*. John Wiley, Chichester, England ; Hoboken, NJ, 2007; pp. x, 306 p.
31. Shao, Z. P.; Yang, W. S.; Cong, Y.; Dong, H.; Tong, J. H.; Xiong, G. X., Investigation of the permeation behavior and stability of a Ba_{0.5}Sr_{0.5}Co_{0.8}Fe_{0.2}O_{3-delta} oxygen membrane. *Journal of Membrane Science* 2000, 172 (1-2), 177-188.
32. Igi, R.; Yoshioka, T.; Ikuhara, Y. H.; Iwamoto, Y.; Tsuru, T., Characterization of co-doped silica for improved hydrothermal stability and application to hydrogen separation membranes at high temperatures. *Journal of the American Ceramic Society* 2008, 91 (9), 2975-2981.
33. Polfus, J. M.; Xing, W.; Fontaine, M. L.; Denonville, C.; Henriksen, P. P.; Bredesen, R., Hydrogen separation membranes based on dense ceramic composites in the La₂W₅O_{55.5}-LaCrO₃ system. *Journal of Membrane Science* 2015, 479, 39-45.
34. Patricio, S. G.; Papaioannou, E.; Zhang, G.; Metcalfe, I. S.; Marques, F. M. B., High performance composite CO₂ separation membranes. *Journal of Membrane Science* 2014, 471, 211-218.
35. Agarwal, A.; Pujari, M.; Uppaluri, R.; Verma, A., Preparation, optimization and characterization of low cost ceramics for the fabrication of dense nickel composite membranes. *Ceramics International* 2013, 39 (7), 7709-7716.
36. Kaniganti, C. M.; Emani, S.; Thorat, P.; Uppaluri, R., Microfiltration of Synthetic Bacteria

Solution Using Low Cost Ceramic Membranes. *Separation Science and Technology* 2015, 50 (1), 121-135.

37. Nandi, B. K.; Uppaluri, R.; Purkait, M. K., Preparation and characterization of low cost ceramic membranes for micro-filtration applications. *Applied Clay Science* 2008, 42(1-2), 102-110.
38. Vasanth, D.; Pugazhenti, G.; Uppaluri, R., Fabrication and properties of low cost ceramic microfiltration membranes for separation of oil and bacteria from its solution. *Journal of Membrane Science* 2011, 379 (1-2), 154-163.
39. Emani, S.; Uppaluri, R.; Purkait, M. K., Microfiltration of oil-water emulsions using low cost ceramic membranes prepared with the uniaxial dry compaction method. *Ceramics International* 2014, 40 (1), 1155-1164.
40. Jedidi, I.; Saidi, S.; Khmakem, S.; Larbot, A.; Elloumi-Ammar, N.; Fourati, A.; Charfi, A.; Ben Amar, R., New ceramic microfiltration membranes from mineral coal fly ash. *Arabian Journal of Chemistry* 2009, 2 (1), 31-39.
41. Belibi, P. B.; Nguemtchouin, M. M. G.; Rivallin, M.; Nsami, J. N.; Sieliechi, J.; Cerneaux, S.; Ngassoum, M. B.; Cretin, M., Microfiltration ceramic membranes from local Cameroonian clay applicable to water treatment. *Ceramics International* 2015, 41 (2), 2752-2759.
42. Wang, Z.; Chen, Z. L.; Chang, J.; Shen, J. M.; Kang, J.; Yang, L.; Chen, Q., A novel cementitious microfiltration membrane: mechanisms of pore formation and properties for water permeation. *Rsc Advances* 2015, 5 (1), 99-108.
43. Nandi, B. K.; Das, B.; Uppaluri, R.; Purkait, M. K., Microfiltration of mosambi juice using low cost ceramic membrane. *Journal of Food Engineering* 2009, 95 (4), 597-605.
44. Buekenhoudt, A., Stability of porous ceramic membranes. In *Inorganic Membranes: Synthesis, Characterization and Applications*, Mallada, R.; Menendez, M., Eds. Elsevier Science Bv: Amsterdam, 2008; Vol. 13, pp 1
45. Choi, H.; Stathatos, E.; Dionysiou, D. D., Photocatalytic TiO₂ films and membranes for the development of efficient wastewater treatment and reuse systems. *Desalination* 2007, 202 (1-3), 199-206.
46. Bae, T. H.; Tak, T. M., Effect of TiO₂ nanoparticles on fouling mitigation of ultrafiltration membranes for activated sludge filtration. *Journal of Membrane Science* 2005, 249(1-2), 1-8.
47. Bosc, F.; Ayrat, A.; Guizard, C., Mesoporous anatase coatings for coupling membrane separation and photocatalyzed reactions. *Journal of Membrane Science* 2005, 265 (1-2), 13-19.
48. Athanasekou, C. P.; Romanos, G. E.; Katsaros, F. K.; Kordatos, K.; Likodimos, V.; Falaras, P., Very efficient composite titania membranes in hybrid ultrafiltration/photocatalysis

water treatment processes. *Journal of Membrane Science* 2012, 392, 192-203.

49. Wang, W. Y.; Irawan, A.; Ku, Y., Photocatalytic degradation of Acid Red 4 using a titanium dioxide membrane supported on a porous ceramic tube. *Water Research* 2008, 42 (19), 4725-4732.
50. Madaeni, S. S.; Ghaemi, N.; Alizadeh, A.; Joshaghani, M., Influence of photo-induced superhydrophilicity of titanium dioxide nanoparticles on the anti-fouling performance of ultrafiltration membranes. *Applied Surface Science* 2011, 257 (14), 6175-6180.
51. Hurum, D. C.; Agrios, A. G.; Gray, K. A.; Rajh, T.; Thurnauer, M. C., Explaining the enhanced photocatalytic activity of Degussa P25 mixed-phase TiO₂ using EPR. *Journal of Physical Chemistry B* 2003, 107 (19), 4545-4549.
52. Bai, H. W.; Liu, L.; Liu, Z. Y.; Sun, D. D., Hierarchical 3D dendritic TiO₂ nanospheres building with ultralong 1D nanoribbon/wires for high performance concurrent photocatalytic membrane water purification. *Water Research* 2013, 47 (12), 4126-4138.
53. Grosso, D., How to exploit the full potential of the dip-coating process to better control film formation. *Journal of Materials Chemistry* 2011, 21 (43), 17033-17038.
54. Kim, T. H.; Sohn, B. H., Photocatalytic thin films containing TiO₂ nanoparticles by the layer-by-layer self-assembling method. *Applied Surface Science* 2002, 201 (1-4), 109-114.
55. Hattori, H., Two-step assembly technique for preparation of polymer-particle composite films. *Thin Solid Films* 2001, 385 (1-2), 302-306.
56. Dotzauer, D. M.; Dai, J. H.; Sun, L.; Bruening, M. L., Catalytic membranes prepared using layer-by-layer adsorption of polyelectrolyte/metal nanoparticle films in porous supports. *Nano Letters* 2006, 6 (10), 2268-2272.
57. Choi, H.; Stathatos, E.; Dionysiou, D. D., Photocatalytic TiO₂ films and membranes for the development of efficient wastewater treatment and reuse systems. *Desalination* 2007, 202 (1-3), 199-206.
58. Choi, H.; Sofranko, A. C.; Dionysiou, D. D., Nanocrystalline TiO₂ photocatalytic membranes with a hierarchical mesoporous multilayer structure: Synthesis, characterization, and multifunction. *Advanced Functional Materials* 2006, 16 (8), 1067-1074.
59. Sobczyk-Guzenda, A.; Pietrzyk, B.; Szymanowski, H.; Gazicki-Lipman, M.; Jakubowski, W., Photocatalytic activity of thin TiO₂ films deposited using sol-gel and plasma enhanced chemical vapor deposition methods. *Ceramics International* 2013, 39 (3), 2787-2794.
60. Julbe, A.; Rouessac, V.; Durand, J.; Ayrat, A., New approaches in the design of ceramic and hybrid membranes. *Journal of Membrane Science* 2008, 316 (1-2), 176-185.
61. Chang, Q. B.; Zhou, J. E.; Wang, Y. Q.; Liang, J.; Zhang, X. Z.; Cerneaux, S.; Wang, X.;

- Zhu, Z. W.; Dong, Y. C., Application of ceramic microfiltration membrane modified by nano-TiO₂ coating in separation of a stable oil-in-water emulsion. *Journal of Membrane Science* 2014, 456, 128-133.
62. Geesey, G. G.; Lewandowski, Z.; Flemming, H.-C., Biofouling and biocorrosion in industrial water systems. Lewis Publishers: Boca Raton, 1994; p 297 p.
63. Ciston, S.; Lueptow, R. M.; Gray, K. A., Controlling biofilm growth using reactive ceramic ultrafiltration membranes. *Journal of Membrane Science* 2009, 342 (1-2), 263-268.
64. Kovaleva, O. V.; Duka, G. G.; Kovalev, V. V.; Ivanov, M. V.; Dragalin, I. P., Membrane photocatalytic destruction of benzothiazoles in an aqueous medium. *Journal of Water Chemistry and Technology* 2009, 31 (5), 297-304.
65. Molinari, R.; Mungari, M.; Drioli, E.; Di Paola, A.; Loddo, V.; Palmisano, L.; Schiavello, M., Study on a photocatalytic membrane reactor for water purification. *Catalysis Today* 2000, 55 (1-2), 71-78.
66. Zhang, H. M.; Quan, X.; Chen, S.; Zhao, H. M.; Zhao, Y. Z., The removal of sodium dodecylbenzene sulfonate surfactant from water using silica/titania nanorods/nanotubes composite membrane with photocatalytic capability. *Applied Surface Science* 2006, 252 (24), 8598-8604.
67. Buser, H. R.; Balmer, M. E.; Schmid, P.; Kohler, M., Occurrence of UV filters 4-methylbenzylidene camphor and octocrylene in fish from various swiss rivers with inputs from wastewater treatment plants. *Environmental Science & Technology* 2006, 40 (5), 1427-1431.
68. Hu, A. M.; Zhang, X.; Oakes, K. D.; Peng, P.; Zhou, Y. N.; Servos, M. R., Hydrothermal growth of free standing TiO₂ nanowire membranes for photocatalytic degradation of pharmaceuticals. *Journal of Hazardous Materials* 2011, 189 (1-2), 278-285.
69. Kummerer, K., The presence of pharmaceuticals in the environment due to human use - present knowledge and future challenges. *Journal of Environmental Management* 2009, 90 (8), 2354-2366.
70. Choi, J.; Lee, H.; Choi, Y.; Kim, S.; Lee, S.; Choi, W.; Lee, J., Heterogeneous photocatalytic treatment of pharmaceutical micropollutants: Effects of wastewater effluent matrix and catalyst modifications. *Applied Catalysis B-Environmental* 2014, 147, 8-16.
71. McCullagh, C.; Robertson, J. M. C.; Bahnemann, D. W.; Robertson, P. K. J., The application of TiO₂ photocatalysis for disinfection of water contaminated with pathogenic micro-organisms: a review. *Research on Chemical Intermediates* 2007, 33 (3-5), 359-375.
72. Rincon, A. G.; Pulgarin, C., Photocatalytical inactivation of *E. coli*: effect of (continuous-intermittent) light intensity and of (suspended-fixed) TiO₂ concentration. *Applied Catalysis B-Environmental* 2003, 44 (3), 263-284.

CHAPTER 2

Comparison of sub mono-layer and dense photocatalytic coating techniques for fabrication of photocatalytic membrane supports

2.1 Introduction

Titanium dioxide (TiO_2) photocatalysis for application in environmental treatment and remediation has been an active area of research due to the ability of the highly reactive oxygen species generated during exposure to UV light to mineralize organic pollutants [1-2]. While TiO_2 photocatalytic processes have seen commercial adoption in fields such as air purification, photocatalytic processes face many challenges in water treatment [3]. Photocatalytic water treatment processes with TiO_2 are often categorized by whether the catalyst is suspended or immobilized [4]. While benefiting from an increased loading, suspended reactors require additional separation units for catalyst recovery. Immobilized photocatalytic catalytic reactors have lower catalytic loadings and limited contact times. In water treatment, combining membrane separation and photocatalysis into a single process unit yields several synergisms. In this area, research has focused on coupling the selective and catalytic functionalities, where the catalyst is integrated into the selective layer of the membrane [5]. This results in pollutant concentration on the catalyst and a reduction in membrane fouling.

Creating photocatalytic coatings on the membrane's support has not been studied extensively. The only publications on the subject are by the groups of Bosc [6] and Athanasekou [7]. This coating configuration has several benefits not available to coupled membranes. First, it allows the optimization of both the photocatalytic and separation functionalities independently. Also,

due to the membranes ability to remove turbidity causing particles, the permeate stream may have increased transparency and therefore afford a higher photocatalytic efficiency. Lastly, coating the membrane's support creates two independent barriers to pollution, which increases process robustness. Whereas with coupled membranes, the photocatalysis and membrane separation are combined and act as one barrier, so that a failure in the catalyst layer results in a loss of both photocatalysis and separation.

Various thin film technologies have been used to create photocatalytic coatings, including dip coating, LbL self-assembly, sol gel, and chemical vapor deposition (CVD) [8-11]. Recently, plasma enhanced chemical vapor deposition (PECVD) was used to create thin films at low temperatures [12]. This reduces energy demand compared with traditional CVD processes and also allows for deposition on temperature sensitive materials. LbL self-assembly has been applied to create various TiO_2 film morphologies, but to date has not been applied on porous ceramic membranes. As illustrated in Figure 2, the objective of this work is to investigate the generation of sub-mono layer TiO_2 layers, on membrane support structures, using LbL self-assembly, with the goal to create photocatalytic membranes with no decrease in membrane permeability. This work will compare the performance in permeability and photocatalytic experiments of an LbL coated membrane to one prepared with PECVD techniques.

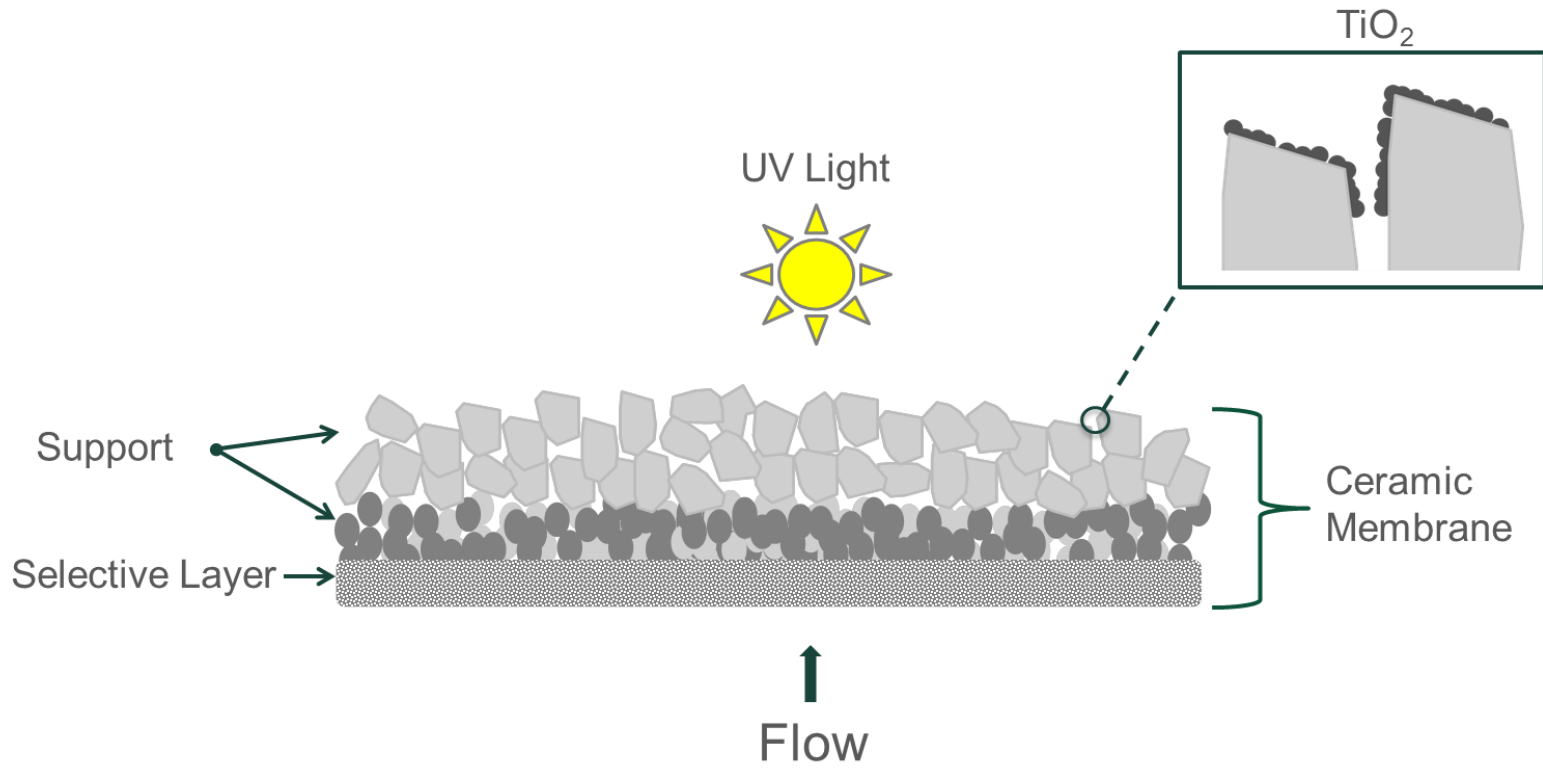


Figure 2: Side view of an asymmetric ceramic membrane with a support photocatalytic layer of TiO₂

2.2 Approach

2.2.1 Fabrication of photoactive membrane layer

LbL self-assembly exploits the surface charge of polyelectrolytes to adhere suspended catalytic nanoparticles to a surface. This involves a two-step process of i) applying polyelectrolytes to the surface, and then ii) exposing the polyelectrolyte-modified surface to a nanoparticle suspension to enable particle-polyelectrolyte adhesion and surface coating of nanoparticles. The morphology of the resulting coating is dependent on the deposition conditions (e.g. pH and ionic strength of the deposition catalyst suspension, the degree of polyelectrolyte ionization) and properties of surfaces involved (e.g. the charge and hydrophilicity of nanoparticles and the membrane). The amount of catalyst surface aggregation is a balance between the like-like repulsion of the catalyst particles and the attractive force between the negatively charged terminating polyelectrolyte and the positively charged catalyst. Manipulation of PE-catalyst interaction was performed by varying the degree of polyelectrolyte ionization and charge of the particle.

PECVD has been developed by Professor André Ayral's research group at the European Institute of Membranes (IEM) [12] as a means of creating dense TiO₂ layers. This method uses chemical vapor deposition techniques with the aid of plasma to oxidize titanium dioxide precursors on a substrate. The parameters used in this experiment have been previously optimized at IEM to create thick and dense coatings [12].

2.2.2 Important elements of photocatalytic membrane layers

Both fabrication methods were applied to the same membrane, allowing for interesting comparisons. PECVD created dense skin coatings, while the objective of the LbL self-assembly was to create sub-mono layer coatings. Additionally, the LbL self-assembly used a commercially available photocatalyst with a known high photoactivity, while the PECVD used catalyst precursors to deposit catalyst in-situ. The approach of this study was to use batch reactions with a model pollutant (Methylene Blue (MB)) to determine the photoactivity of each catalyst and evaluate degradation of the same pollutant in a photocatalytic membrane reactor to lend insight into the coating quality.

The removal of MB is dependent on both the concentration of MB and the concentration of reactive oxygen species, ROS (eq. 1). Assuming the reactive oxygen specie concentration is constant (eq. 2), the reaction simplifies to pseudo-first order (eq. 3), which can be measured in a batch reactor.

$$1. \quad \frac{dMB}{dt} = K[MB][ROS]$$

$$2. \quad k' = K[ROS]$$

$$3. \quad \frac{dMB}{dt} = k'[MB]$$

The ROS concentration is a product of the catalyst yield, Y (mol ROS/m²), and the specific surface area, S (m²/L), of photocatalyst in the reactor. Plugging these constants into eq. 2 and defining k'' (m/s) as a product of K and Y , results in eq. 6.

$$4. \quad [ROS] = Y * S$$

$$5. \quad k' = K * Y * S$$

$$6. \quad k'' = \frac{k'_{batch}}{S_{batch}} = k'_{batch} * \frac{V_{batch} * r * \rho_{TiO_2}}{3 * M_{TiO_2}}$$

where k' is the pseudo-first order reaction constant measured in a batch reactor, V_{batch} is the volume of the batch reactor, r is the radius of the spherical catalyst particle, and M_{TiO_2} is the total mass of catalyst in the reactor.

To find the plug flow reaction constant, k'' is multiplied by specific surface area, S_{PFR} , of catalyst in the reactive zone of the PFR. The reactive zone is defined as the area where both catalyst and UV light are available. Setting Θ as the relative surface area of the catalyst to the total pore surface area in the reactive zone simplifies the equation.

$$7. \quad k_{pf} = k'' * S_{PFR} = k'' * \frac{4 * \Theta}{d_{pore}}$$

The slope of the linearized plug flow equation, k_{pf} , can be measured using UV-dead-end filtration experiments, where τ is residence time (eq. 8). By assuming a cylindrical reactive pore shape with a specific reactor length, residence time is given by the product of membrane cross-sectional area, A , porosity, ϕ , the length of the reactive zone, $l^{reactive}$, and the inverse of flowrate, Q^{-1} . By plotting experimental results against the inverse of flowrate, the product of k_{pf} and $A\phi l^{reactive}$, shown as η , can be determined. This term is referred to as reactive flux.

$$8. \quad \ln\left(\frac{C}{C_0}\right) = k_{pf}\tau = k_{pf}A\phi l^{reactive} * \left(\frac{1}{Q}\right)$$

$$9. \quad \eta = k_{pf}A\phi l^{reactive}$$

Using equations 7 and 9, a ratio can be taken between two coating techniques. With the use of the same membrane, the cross-sectional area, porosity, and pore diameter are equal, leaving eq. 10. Here we can see the importance of both a long reactive zone and a dense coating to in creating a highly efficient photocatalytic reactor. A ratio greater than 1 indicates the LbL method has a higher quality coating and less than 1 indicates PECVD resulted in a better coating with this membrane. Herein high quality refers to both higher amount of catalyst surface area and optimal placement of the catalyst. The length of the reactive zone is a function of pore morphology and depth of coating. By using the same membrane, the relative parameters, l and Θ , are attributed solely to the coating technique. The constants used in this approach are summarized in Table 2.

$$10. \quad \frac{l_{LbL} * \Theta_{LbL}}{l_{PECVD} * \Theta_{PECVD}} = \frac{(\eta)_{LbL}}{k''_{LbL}} * \frac{k''_{PECVD}}{(\eta)_{PECVD}}$$

Table 2: Summary of constants used in approach

| Constant | Units | Description |
|---|---------------------------------|---|
| K | $L \cdot mol^{-1} \cdot s^{-1}$ | Overall reaction constant for the degradation of methylene blue by reactive oxygen species |
| k' | s^{-1} | Product of [ROS] and K, pseudo-first order reaction constant |
| k'' | $L \cdot s^{-1} \cdot m^{-2}$ | k' normalized by the specific surface area of TiO_2 in the reactor |
| η | $min \cdot L^{-1}$ | Reactive flux, slope of $\ln(C/Co)$ vs $1/Q$, where C is concentration of methylene blue |
| Q | $L \cdot min^{-1}$ | Flowrate through membrane |
| l | m | Length of reactive area in pore |
| A | m^2 | Cross-sectional area of membrane |
| Θ | Dimensionless | Ratio of catalyst surface area in pore to total pore wall area in reactive zone |
| $\frac{l_{LbL} \cdot \Theta_{LbL}}{l_{PECVD} \cdot \Theta_{PECVD}}$ | Dimensionless | Coating quality ratio, value larger than 1 indicates LbL results in a higher quality coating. Value less than 1 indicates PECVD yields a higher quality coating |

2.3 Experimental

2.3.1 Reagents

Polyelectrolytes used for the LbL deposition of catalyst included reagent grade polydiallyldimethylammonium chloride (Aldrich, MW 100,000-200,000), polyacrylic acid (Aldrich, MW 1,800), poly(sodium styrene sulfonate) (Aldrich, MW 70,000), and poly(allylamine hydrochloride) (Aldrich, MW 70,000). Commercially available titanium dioxide (Degussa P25) was used as a catalyst in all LbL self-assembly coatings. Titanium tetra-isopropoxide (TTIP) (Sigma-Aldrich) was used as a precursor in plasma enhanced chemical vapor deposition coatings. Methylene blue (Sigma) was used as a model pollutant in both batch and photocatalytic filtration experiments. Potassium iodine (Jade Scientific), iodate (EM Industries), and borate buffer (Sigma-Aldrich) solutions were used in chemical actinometry to quantify UV fluence [13, 14]. All membranes were cleaned in nitric acid (EMD Performance Materials) and sodium hydroxide (Sigma-Aldrich) solutions. Glass slides were cleaned with detergent (Alconox), hydrochloric acid (EDM Performance Materials), and acetone (Sigma-Aldrich). Piranha solution was prepared with a mixture of sulfuric acid (J.T. Baker) and hydrogen peroxide (Fisher Scientific). Additionally, hydrochloric acid (EMD Performance Materials) and sodium hydroxide (Sigma-Aldrich) were used for pH adjustments.

2.3.2 LbL assembly

LbL self-assembly involves a two-step coating process. First the polyelectrolytes are coated on a substrate to modify the surface charge and then the polyelectrolyte-coated substrate is dipped in

suspended catalyst to adhere catalyst particles. Initial LbL deposition was performed on glass slides (VWR, 24x60 mm). The slides were cleaned by consecutively sonicating in solutions of detergent, hydrochloric acid, and acetone. After cleaning, the slides were oxidized with a 3:1 mixture of sulfuric acid and hydrogen peroxide. The clean slides were alternately dip coated in anionic and cationic 0.02 M solutions of polyelectrolytes. After each layer of polyelectrolyte, the samples were rinsed with DI water. The two polyelectrolyte systems used were PAH&PSS and PDADMAC&PAA. With both systems, cationic polyelectrolytes were used as initiating layers and anionic polyelectrolytes were used as the terminating layer. A complete coating of polyelectrolytes consisted of 4 bilayers, with each bilayer having 1 anionic and 1 cationic polyelectrolyte. After coating 4 bilayers of polyelectrolytes, the glass slides were dried in a gentle stream of compressed air. The polyelectrolyte coated slides were then submerged in a 300 mg/L suspension of Degussa P25 photocatalyst for 30 minutes. To prepare the catalyst suspension, the TiO₂ was suspended in DI water and sonicated using a bath sonicator. Prior to sonication, the pH of the catalyst suspension was adjusted to match the pH of the terminating polyelectrolyte layer. Both 0.01 M and 0 M ionic strength catalyst suspensions were used for investigation of double layer charge compression effects on deposited catalyst morphology.

Flat disc ceramic membranes (TAMI Industries, FR) with a 0.14 μm pore size were used for fabrication of LbL self-assembled photocatalytic membranes. The membranes were cleaned prior to coating by soaking for 30 minutes in 20 g/L sodium hydroxide at 80°C, followed by soaking for 15 minutes in 5 ml/L nitric acid. The first LbL membrane was prepared with 4 bilayers of PDADMAC&PAA and 1 layer TiO₂. The pH of the PAA solution and TiO₂ were adjusted to 5 and the TiO₂ suspension had 0 M ionic strength. Additionally, a second membrane was prepared with 5 total layers of TiO₂ by repeating the alternating layers of

(PDADMAC&PAA)₄ and TiO₂. During coating, only the support structure of the membrane was exposed to polyelectrolytes and catalyst. Following deposition of catalyst, the membranes were sintered at 500°C for 45 minutes (RHF 15/3, Carbolite Ltd).

2.3.3 Plasma enhanced chemical vapor deposition

Photocatalytic membranes fabricated with PECVD were prepared using the same flat disc ceramic membranes used with the LbL technique. Membranes were coated at the European Institute of Membranes, using a process previously developed and optimized [12]. Prior to the deposition of catalyst, the membranes were cleaned by soaking for 30 minutes in 20 g/L sodium hydroxide at 80°C, followed by soaking for 15 minutes in 5 ml/L nitric acid. The membrane was then placed in the deposition chamber and a vacuum was applied. The membrane was heated to 150°C throughout deposition. Using argon as a carrier gas, titanium tetra-isopropoxide (TTIP) was feed to the chamber along with oxygen. The flux ratio of TTIP to oxygen had been previously optimized for maximum coating thickness and homogeneity. The carrier gas line was heated to 100°C to prevent condensation of precursor. An R.F. induced plasma was applied for 20 minutes, resulting in the formation of titanium dioxide catalyst on the substrate. The deposition process was repeated to create 1 and 2 layer PECVD coated membranes. During deposition, only the membrane support was exposed to PECVD.

2.3.4 Batch experiments

The photocatalytic efficiency of P25 and PECVD generated catalysts were measured in a UV batch reactor. The batch reactor consisted of a UV exposure box, UV lamp (16 W, model GPH330T5L/4, Atlantic Ultraviolet Corp), stir plate, and a beaker (Figure 3B). The UV lamp emitted within the germicidal range, with 95% of emitted energy at the 254 nm wavelength. Batch experiments with P25 and PECVD generated catalysts were conducted using MB as a model pollutant. The catalyst suspension was prepared by suspending catalyst particles in DI water and adjusting the pH using HCl. The Degussa P25 suspension had pH 4 and the PECVD generated catalyst had pH 3.1. MB was added to the catalyst suspensions and allowed to equilibrate for 30 minutes prior to UV exposure. During the batch test, the fluid remained stirred and samples were taken at periodic intervals of UV exposure.

To prepare PECVD generated catalyst powder, thin layers of catalyst were deposited on silicon wafers and sintered at 500°C for 1 hour. Using a micro-spatula, the coatings were then scraped to generate loose powder. This powder was suspended with DI water and sonicated for 2 hours. The particle diameters of the suspended catalyst were measured prior to MB experiments (Brookhaven, ZetaPALS).

2.3.5 Dead-end filtration experiments

A UV dead-end filtration test apparatus was constructed by machining a permeate window in a 47 mm diameter stainless steel dead-end filtration cell (Sterlitech). A 1/8" thick quartz glass disc (Technical Glass Products) was fit into the window with a glass hose barb to capture the

permeate stream. During UV dead-end filtration experiments, the membrane holder was positioned such that the permeate window was uniformly exposed to UV light. The dead-end filtration experiments utilized the same UV exposure box and UV lamp as the batch reaction experiments. All dead-end filtration experiments were conducted in the constant pressure regime. The first stage of filtration was performed in the absence of UV until constant a permeate concentration of MB was achieved. After reaching a steady permeate concentration, the permeate was exposed to UV through the quartz window and permeate samples were collected at regular intervals. Flux was recorded using a data acquisition system.

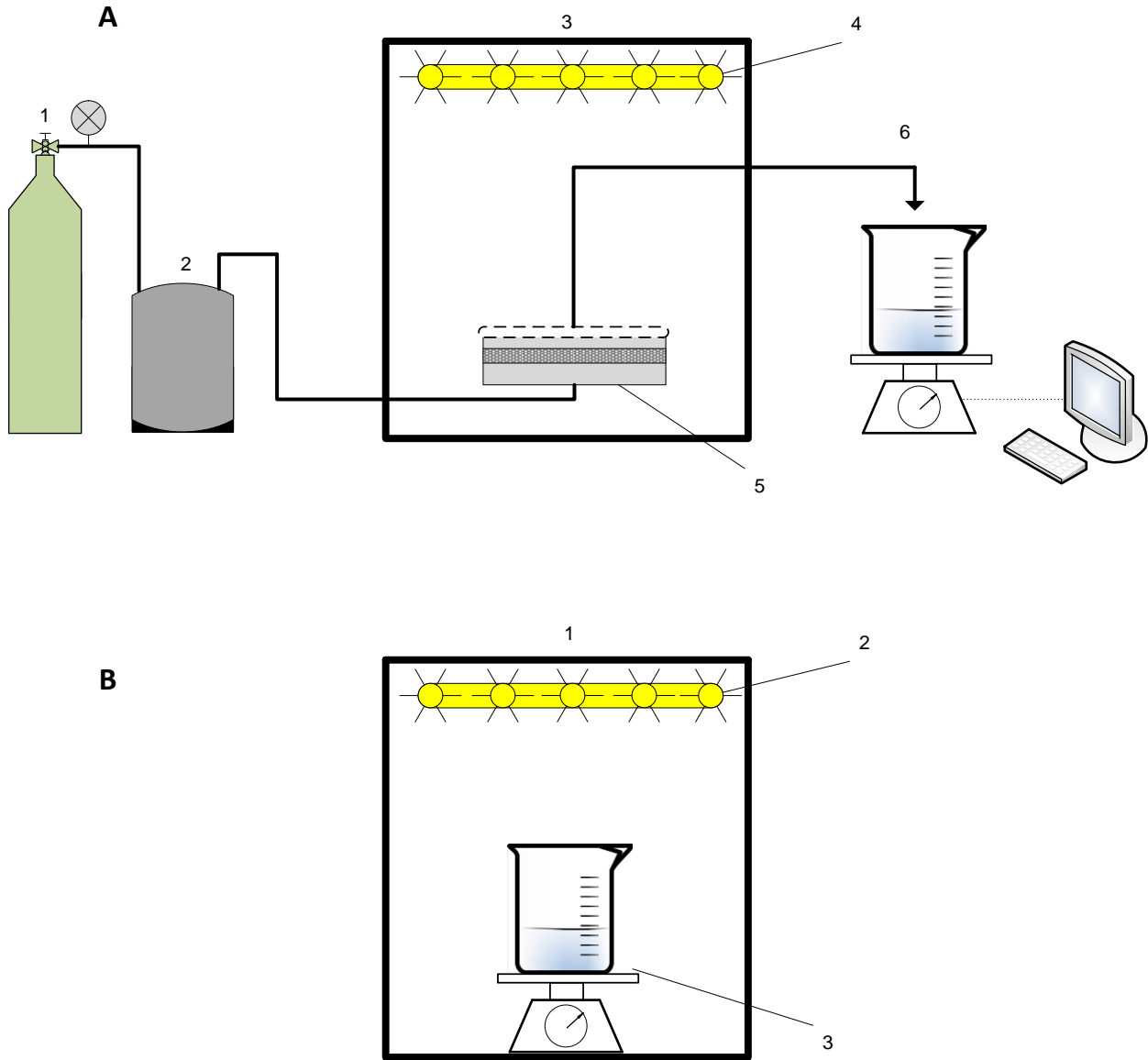


Figure 3: UV-microfiltration test apparatus. A: 1) Compressed air cylinder 2) Stainless steel feed tank 3) UV exposure box 4) Germicidal UV lamp 5) Membrane filtration cell with permeate UV window 6) Collection beaker with data acquisition system B: 1) UV exposure box 2) Germicidal UV lamp 3) Beaker and stir plate.

2.3.6 Measuring concentration of Methylene Blue

Methylene Blue sample absorbance was measured at 663 nm and converted to concentration using the Beer-Lambert Law, eq. 11.

$$11. \quad abs = \epsilon * C_{mb} * l$$

Where ϵ is the extinction coefficient, C_{mb} is the MB molar concentration, and l is the optical path length. An extinction coefficient of $69,362 \frac{L}{mol \text{ cm}}$ at 663 nm was determined by measuring the absorbance (MultiSpec, 1501, Shimadzu) from a series of MB dilutions. The optical path length was 1 cm.

2.3.7 UV fluence quantification

The UV fluence was measured using chemical actinometry. A stock solution of 0.1 M iodate and 0.01 M sodium borate was prepared and the pH was adjusted to 9.25. For each sample, 100 mL of stock solution was added to a beaker with 0.6 M potassium iodide. The quantum yield was calculated according to eq. 12, where T is temperature in Celsius and C is the molar concentration [13]. The sample was placed in the UV exposure box and exposed to UV light while under continuous stirring for a given period of time. The absorbance at 352 nm of an irradiated and non-irradiated baseline sample were measured. The fluence was calculated according to eq. 13 [15].

$$12. \quad \Phi \left(\frac{\text{mol}}{\text{einstein}} \right) = 0.75[1 + 0.02(T - 20.7)][1 + 0.23(C - 0.577)],$$

$$13. \quad F \left(\frac{J}{\text{cm}^2} \right) = \frac{\eta * \Delta A_{352} * V}{\epsilon * S * \Phi},$$

where η is a conversion factor, 4.72×10^5 J/Einstein, ΔA_{352} is the difference in absorbance from the baseline to the irradiated sample at 352 nm, V is the volume of the sample, ϵ is the molar absorption coefficient at 352 nm, 26,400 L/mol, S is the exposed surface area, cm^2 , and Φ is the quantum yield as calculated in eq. 12.

2.3.8 Scanning electron microscope imaging

Scanning electron microscopy (SEM) images of the LbL coated glass slides and membranes were recorded (JEOL 6610LV SEM) under various magnifications. Samples of membrane and glass slides for SEM imaging were obtained by breaking the sample, mounting a piece onto an aluminum stub, and coating the mounted sample with ~ 20 nm thick layer of gold (Emscope Sputter Coater, model SC 500, Quorum Technologies). The sample was then scanned to ensure uniform appearance and images were taken of representative areas.

2.4 Results and Discussion

The experimental parameters are summarized in Table 3. Preliminary results indicated the single layer LbL membrane had limited photoactivity and UV dead-end filtration experiments were not continued with this membrane. Photocatalytic results with methylene blue are reported for the 1

and 2 layer PECVD membranes and the 5 layer LbL membrane. SEM images were taken of 1 LbL coatings on glass slides and membrane pieces.

Table 3: LbL and PECVD experimental parameters

| Coating Technique | Catalyst | Layers of Catalyst | Experiments | Model Pollutant | Imaging |
|---|--------------------------------|--------------------|-------------------|-----------------|--------------------------|
| Layer-by-layer Self-Assembly | Degussa P25 | 1 | -- | -- | Glass Slides Membrane |
| | | 5 | Batch Dead-end | Methylene Blue | -- |
| Plasma Enhanced Chemical Vapor Deposition | PECVD Generated Catalyst | 1 | Batch | Methylene Blue | -- |
| | | 2 | Dead-end | | -- |

2.4.1 Titanium dioxide LbL assembly characterization

The polyelectrolyte systems employed in LbL self-assembly were PAH+PSS and PDADMAC+PAA. A primary difference between the two systems is the degree of dissociation of the terminating polyelectrolyte. PSS is a strong polyelectrolyte and fully dissociated in solution. In contrast, PAA is weak polyelectrolyte and the level of dissociation is dependent on solution pH. Additionally, the initiating polyelectrolytes layers differ. PAH is classified as a weak polyelectrolyte and PDADMAC is a strong polyelectrolyte. Figure 4A shows an image of the (PAH+PSS)₄+TiO₂ coating on a glass slide. The coating technique resulted in a sub-monolayer deposition of TiO₂. With the aid of an image processing software (ImageJ), the deposited particle radius was estimated to be approximately 20 nm. This is slightly larger than reported values for Degussa P25, indicating either measurement error or possibly aggregates consisting of several particles [16]. This morphology is in contrast to previously reported thin

film morphologies of (PAH+PSS)+TiO₂, which showed dense layers of catalyst [17]. This difference may be attributed to the lower pH of the catalyst in our study; a lower pH is expected to increase electrostatic repulsion between catalyst nanoparticles.

The impact of pH on morphology with weak polyelectrolytes is shown in Figure 4C and 4D. The pH of PAA was 2.5 in Figure 4C and 5 in Figure 4D. In both images, the pH of the TiO₂ was matched to PAA. The lower pH system results in a denser coating. Over this pH range the PAA degree of ionization increases from approximately 20% at pH 2.5 to 40% at pH 5 [18]. Since the lower pH results in a denser coating, even with a less ionized polyelectrolyte, the more highly charged catalyst at pH 2.5 appears to be the prevailing force to create denser coatings under these conditions.

During LbL deposition experiments, the morphology is very sensitive to processing parameters, such as sonication. Figures 4E and 4F show the same film with the only difference in assembly being the amount of sonication. Additionally, experiments using a catalyst suspension with a 0.01 M ionic strength resulted in large surface aggregation, Figure 4B.

A ceramic membrane was broken in several pieces and coated with (PDADMAC+PAA)₄+TiO₂, Figure 5, using the same technique as the glass slide in Figure 4D. The PAA solution and TiO₂ were adjusted to pH 5. Compared with the coating on glass slides, the coating on the membrane appears to be more heterogeneous, with both well-coated and barren (i.e. uncoated) areas present. Based on SEM images, the average pore size of the support was measured to be 1.8 μm. Currently, the PECVD membrane coatings have not been imaged.

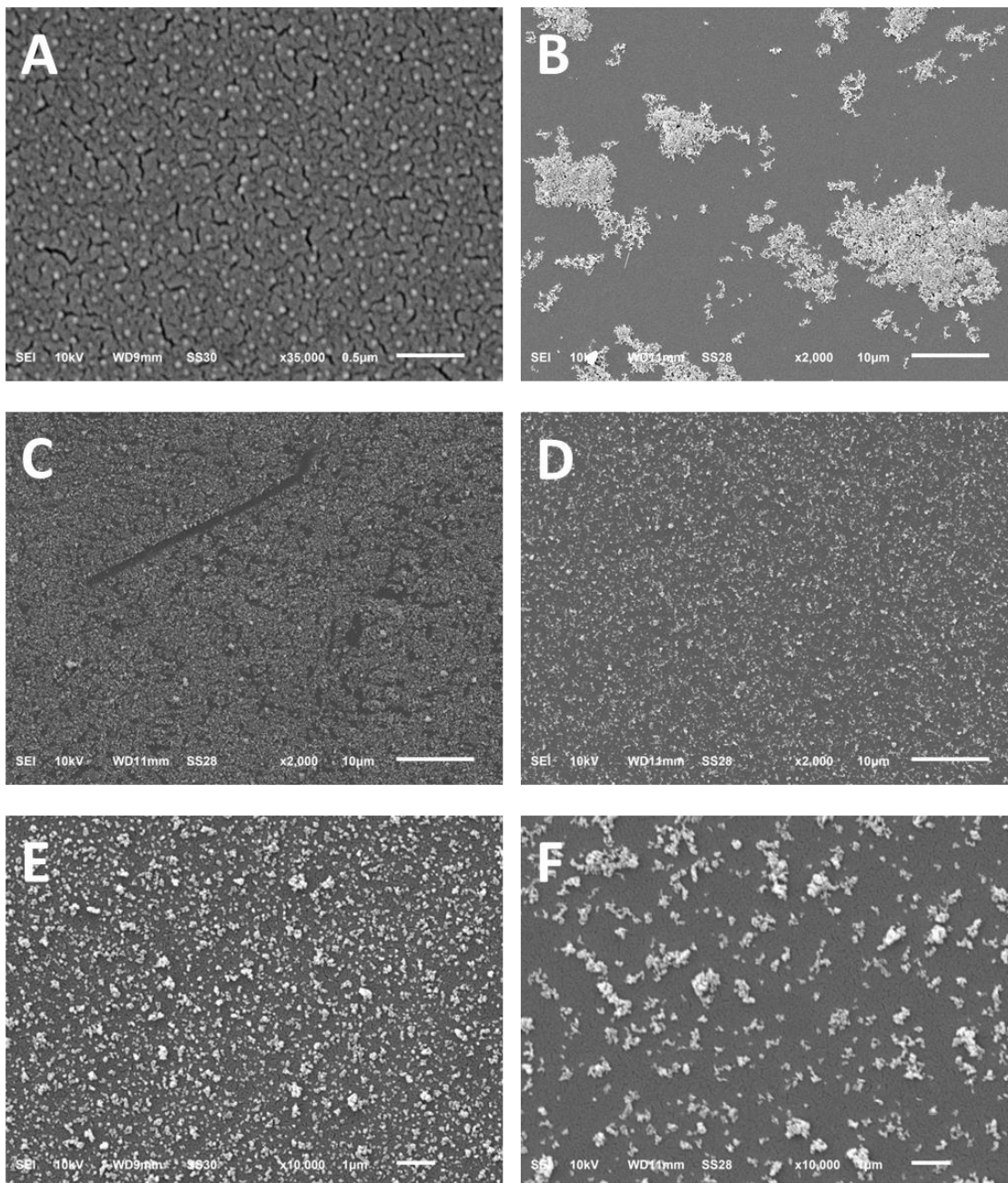


Figure 4: SEM images of LbL assembly of TiO_2 nanoparticles on glass slides:
 A) (PAH+PSS)+ TiO_2 ;
 B) (PDADMAC+PAA)₄+ TiO_2 with catalyst in 0.01 M ionic strength solution;
 C) (PDADMAC+PAA)₄+ TiO_2 with PAA and TiO_2 pH 2.5;
 D) (PDADMAC+PAA)₄+ TiO_2 with PAA and TiO_2 pH 5;
 E) (PDADMAC+PAA)₄+ TiO_2 using high power probe sonicator;
 F) (PDADMAC+PAA)₄+ TiO_2 using bath sonicator.

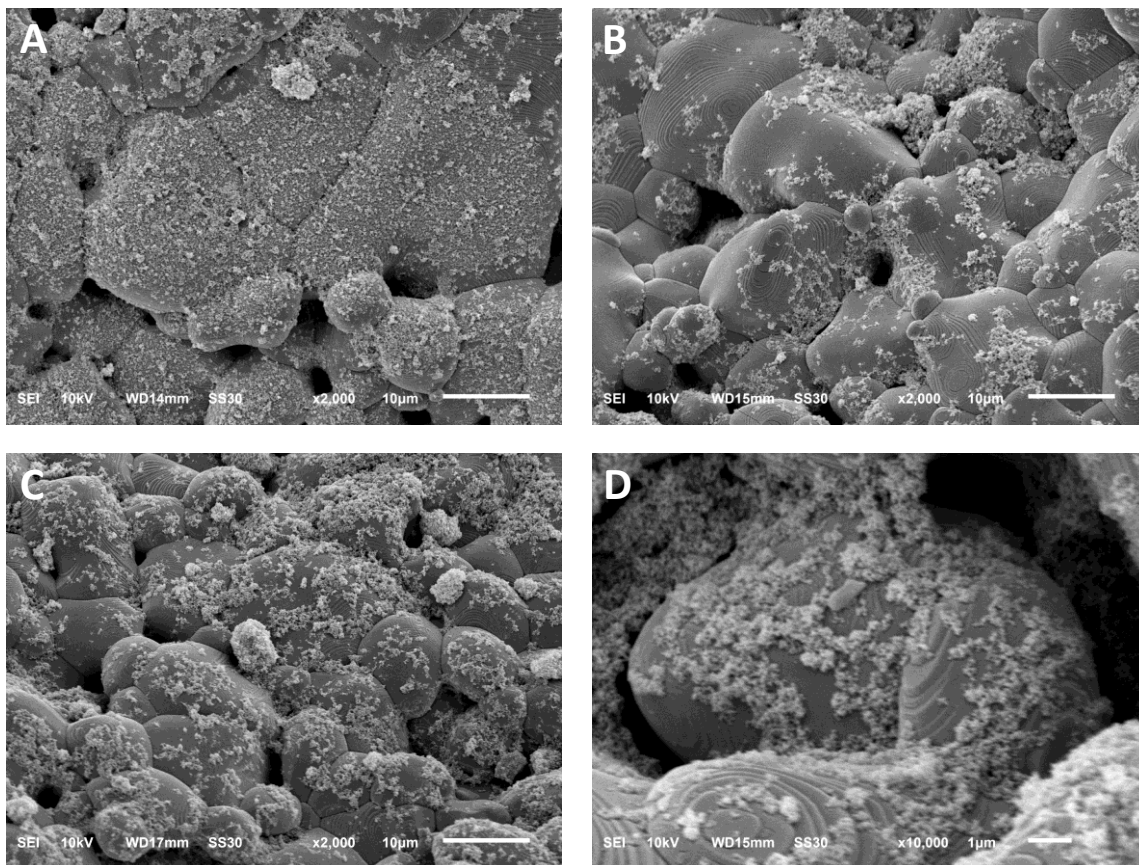


Figure 5: SEM images of $(\text{PDADMAC}+\text{PAA})_4+\text{TiO}_2$ coated ceramic membranes

2.4.2 Batch experiments on photocatalytic oxidation of methylene blue

Batch experiments with MB were performed with Degussa P25, the catalyst used to fabricate the LbL membrane, and PECVD generated catalyst (Figure 6). The initial concentration of MB was approximately 2 mg/L in all experiments. There was limited MB degradation in batch experiments performed without catalyst (-□-, Figure 6). A catalyst loading of 10 mg/L was used in experiments with P25 and 17 mg/L was used for experiments with PECVD. These loadings were chosen to result in a measurable degradation of MB, while not creating an opaque solution that would shield UV. Prior to the addition of MB, the particle size for each catalyst was

measured. The suspended P25 catalyst was 268 ± 14 nm. This is approximately 10 times larger than reported values for individual P25 particles and it is likely that the suspension consisted of aggregated particles. The suspended PECVD catalyst was 6.7 ± 3.3 μm , significantly larger than P25. Both catalytic reactions followed a linear natural log dependence on time, indicating pseudo-first order reaction kinetics. From Figure 6, it appears that P25 is more photocatalytically active than PECVD catalyst, but after normalizing the first order reaction constant by specific surface in the reactor, assuming spherical particles, the two catalysts have a similar photoactivity. The normalized first order reaction constants are $0.008 \pm 0.0015 \frac{\text{L}}{\text{m}^2\text{s}}$ and $0.006 \frac{\text{L}}{\text{m}^2\text{s}}$ for P25 and PECVD generated catalysts, respectively. Batch testing for PECVD generated catalyst was only completed once, due to a limited quantity of powdered catalyst available.

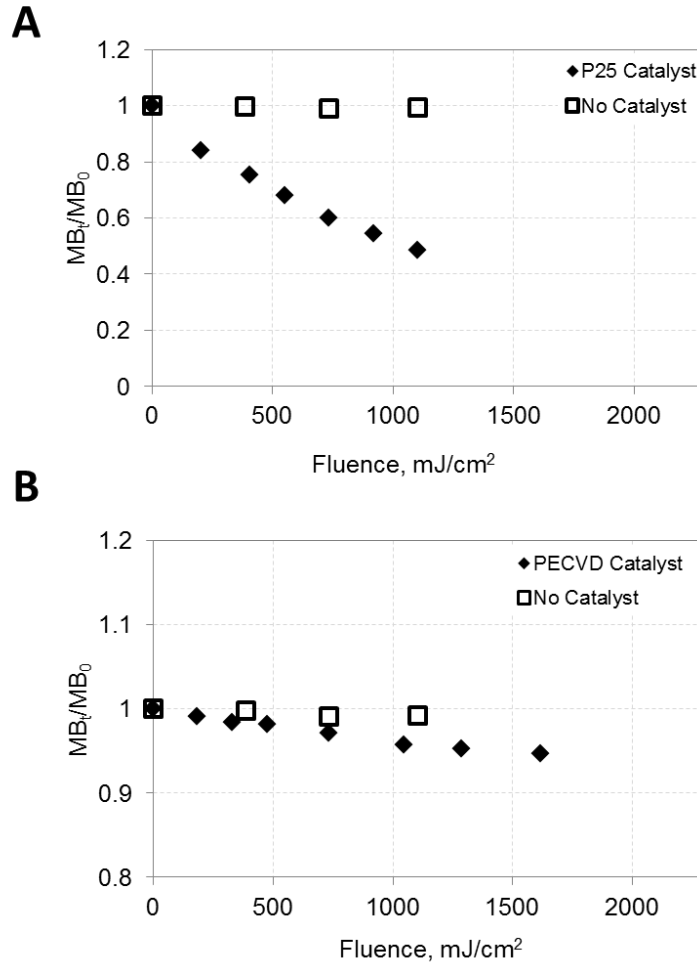


Figure 6: MB batch experiments with A) 10 mg/L Degussa P25 catalyst B) 17 mg/L PECVD generated catalyst

2.4.3 LbL and PECVD layer permeability

The permeability of the membranes before and after applying the LBL and PECVD coatings was compared using a clean water flux test (Figure 7). In all experiments, the membranes permeability decreased with time. As this test was performed with clean DI water, this decrease in permeability for both the coated and uncoated membrane was attributed to permeation-induced changes in the membrane structure, not fouling. In Figure 7A, the 0.14 μm membrane

coated with 5 layers of LbL assembled catalyst exhibits the same permeability to DI water as the membrane before coated. Comparing Figures 7B and 7C shows that both 1 and 2-layer PECVD on 0.14 μm membranes also did not decrease permeability.

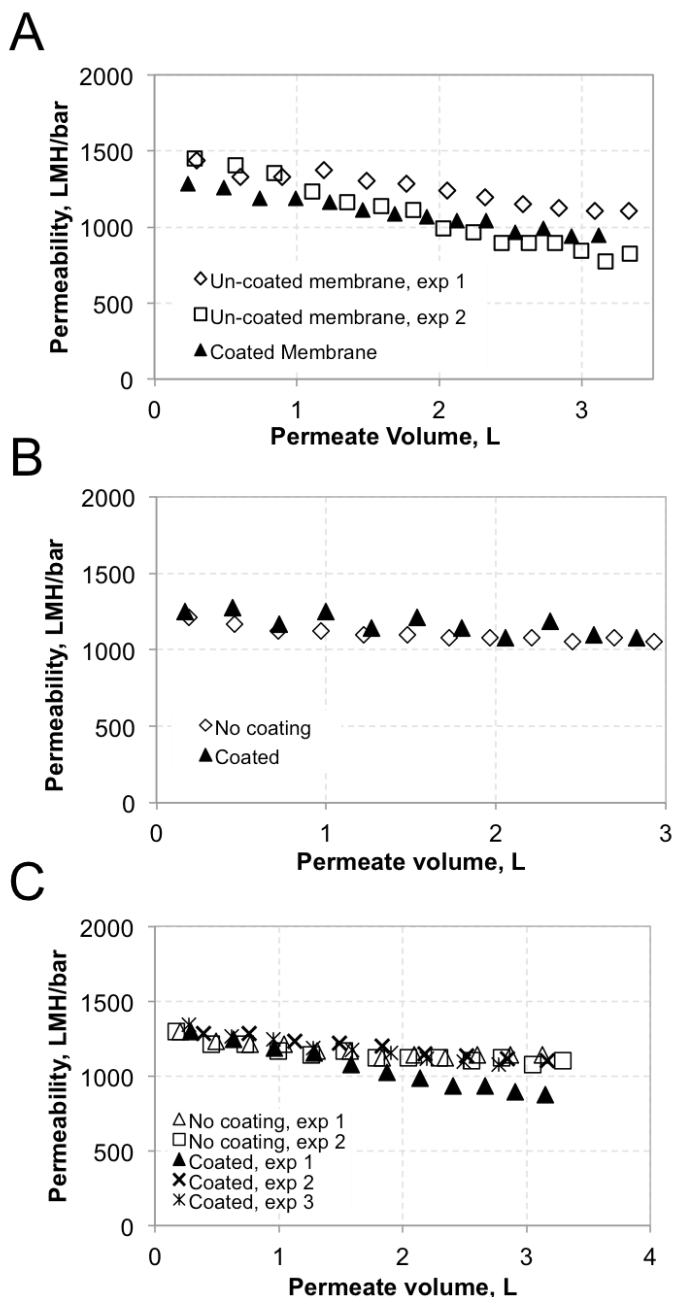


Figure 7: Clean water flux tests with photocatalytic 0.14 μm membranes A) 5-layer LbL; B) 1-layer PECVD; C) 2-layer PECVD.

2.4.4 UV MB dead-end filtration and analysis

Comparison of the photocatalytic efficiency of the PECVD and LbL fabricated membranes was performed using UV dead-end filtration experiments with MB (Figure 8). Each experiment was repeated 3 times under the same conditions and all data are plotted with the linearized plug flow reactor equation (eq. 8). Results are shown for membranes coated with 1 and 2-layers of PECVD and 5-layers of LbL. Experiments show a strong linear dependence when MB degradation is plotted against the inverse of flow rate, which is proportional to residence time. A 95% confidence interval was generated for the linear regression model in comparison to the experimental values (Table 4). From the results, the photocatalytic degradation of MB in the first two experiments with the 5-layer LbL membrane are equivalent, while the third experiment appears significantly lower. This could be indication of poor catalyst adhesion. Comparison of the first and third experiment with the 1-layer PECVD membrane indicates there was not a change in photocatalytic activity during this set of experiments. Similar to the 5-layer LbL, the third experiment of the 2-layer PECVD membrane has a slope significantly less than the first two. Comparing the photocatalytic efficiency of coating technique, with $\alpha = 0.1$, shows that the LbL membrane has a significantly different photocatalytic activity than the 1-layer PECVD membrane. There is not a difference between the 1 and 2-layer PECVD and 2 -layer PECVD and LbL self-assembly.

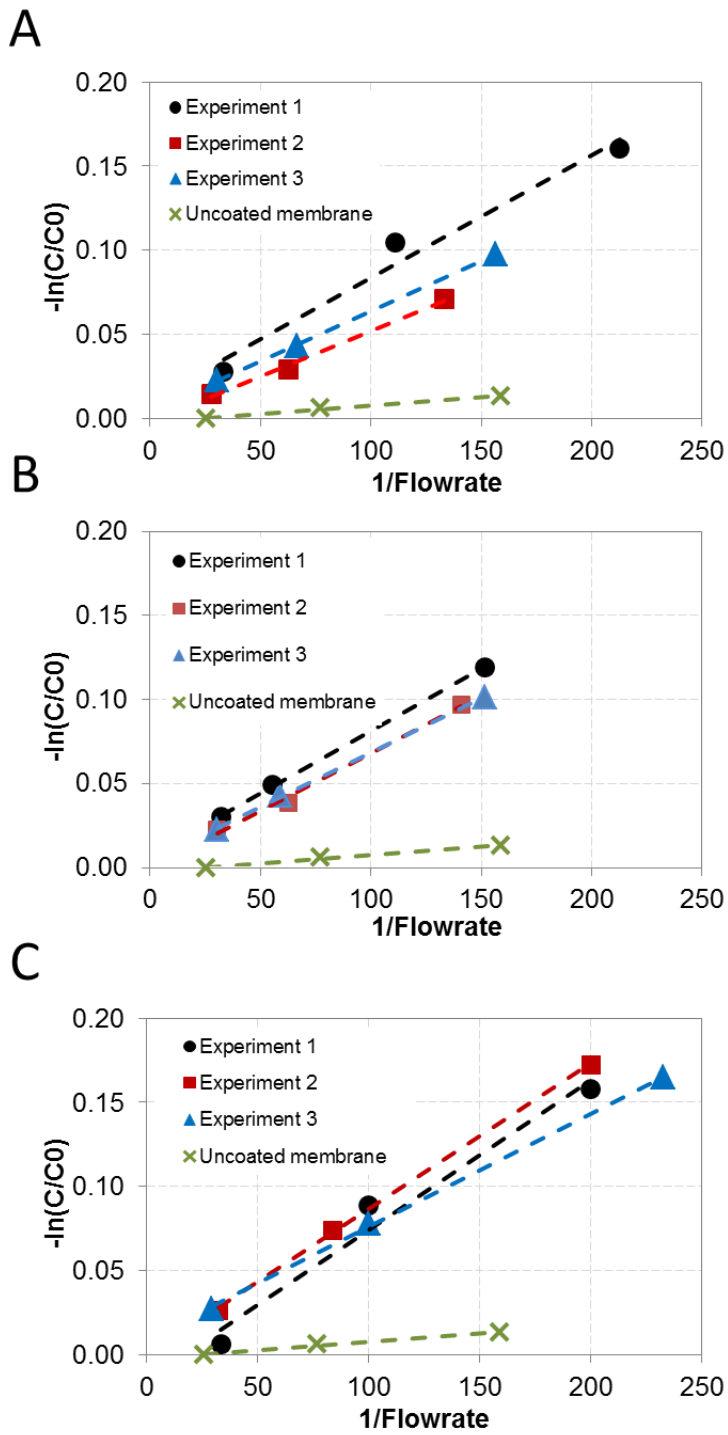


Figure 8: MB UV dead-end filtration experiments A) 0.14 μm , 1 layer PECVD B) 0.14 μm 2 layers PECVD C) 0.14 μm , 5-layer LbL

Table 4: Experimental results of MB UV dead-end filtration experiments

| Experiment | | η | +/- |
|-------------------|---|--------------------------|------------|
| LbL 5 layers | 1 | 8.90E-04 | 2.10E-04 |
| | 2 | 8.66E-04 | 2.72E-05 |
| | 3 | 6.74E-04 | 2.69E-05 |
| PECVD 1 layer | 1 | 7.30E-04 | 1.74E-04 |
| | 2 | 5.42E-04 | 5.72E-05 |
| | 3 | 5.95E-04 | 1.37E-05 |
| PECVD 2 layers | 1 | 7.41E-04 | 2.33E-05 |
| | 2 | 6.82E-04 | 7.66E-05 |
| | 3 | 6.44E-04 | 2.48E-05 |

As shown in Figure 9A, 5-layer LbL self-assembly fabrication resulted in the highest reactive flux, determined according to equation 8. The photocatalytic efficiency of the coating is dependent on how reactive the catalyst is, the amount of catalyst, and its placement. To separate the influence of catalyst reactivity and focus on coating quality, the η/k'' value was calculated for each membrane, where k'' was calculated from batch experiment data (Table 5). When taking the η/k'' ratio between coating techniques, according to equation 10, the coating qualities are all within the propagated error. Since both coating techniques result in a similar coating quality, the improved dead-end-filtration kinetics seen with 5-layer LbL membrane is attributed to the higher catalytic efficiency of Degussa P25.

Table 5: LbL self-assembly and PECVD coating quality

| Coating Technique | η , +/- | | k'' , +/- | | η/k'' , +/- | | $\Theta_x I_x / \Theta_y I_y$, +/- | |
|-------------------|--------------|----------|-------------|----------|------------------|----------|-------------------------------------|----------|
| PECVD: 2 layer | 6.89E-04 | 2.81E-05 | 6.0E-03 | 3.72E-06 | 1.15E-01 | 4.68E-03 | 1.00E+00 | 5.77E-02 |
| PECVD: 1 layer | 6.22E-04 | 5.59E-05 | 6.0E-03 | 3.72E-06 | 1.04E-01 | 9.32E-03 | 9.03E-01 | 8.92E-02 |
| LbL: 5 layers | 8.10E-04 | 6.83E-05 | 7.9E-03 | 7.5E-04 | 1.03E-01 | 1.30E-02 | 8.93E-01 | 1.19E-01 |

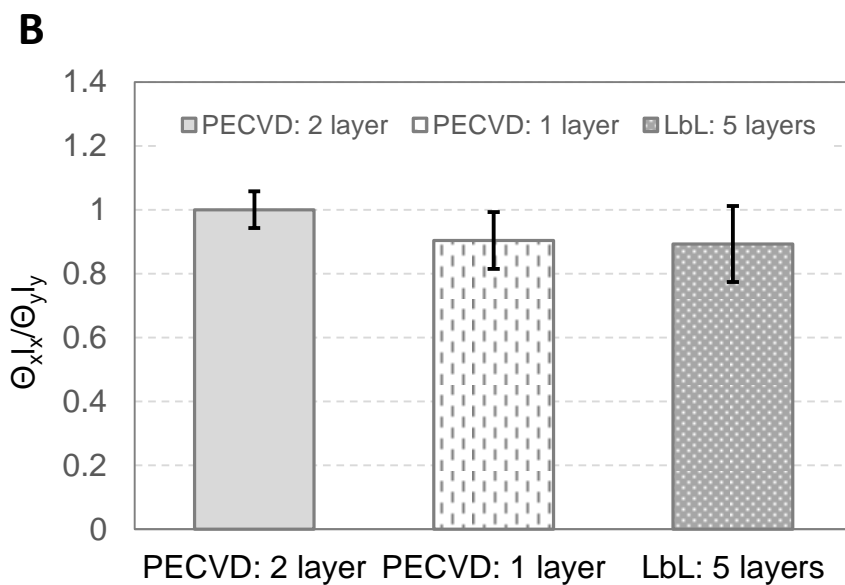
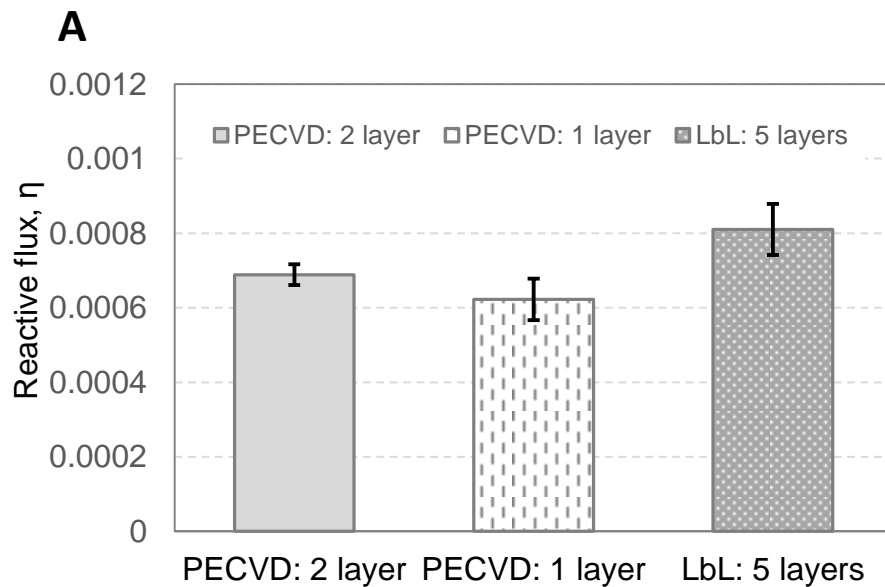


Figure 9: Comparison of Photocatalytic Coatings A) Reactive flux B) $\Theta_x I_x / \Theta_y I_y$, where x is the coating used in the column and y is the PECVD coating with 2 layers

2.5 Conclusion

A sub-mono layer fabrication technique using LbL self-assembly has been developed for deposition of titanium dioxide photocatalyst on ceramic membrane support structures. The resulting photocatalytic layers do not reduce the membrane permeability. In comparison with established PECVD processes, the membrane had a higher overall rate of pollutant removal during UV dead-end filtration experiments. Insight into the relative coating quality was determined by normalizing the dead-end filtration results with catalyst efficiency. This indicated that both coating techniques result in a similar coating-quality and therefore the higher rate of removal seen with LbL self-assembly is attributed to the improved catalyst efficiency of P25. This analysis points to pathways for improving each coating technique. LbL, with its high catalyst efficiency, should target increasing the amount of catalyst in the reactive zone. In contrast, PECVD, with a lower catalyst reactivity, should focus on increasing catalytic efficiency. While this study analyzed two coating techniques using the same substrate, a similar comparison can be made to find the optimal substrate geometry by coating different substrates with the same coating technique.

REFERENCES

REFERENCES

1. Brezova, V.; Jankovicova, M.; Soldan, M.; Blazkova, A.; Rehakova, M.; Surina, I.; Ceppan, M.; Havlinova, B., Photocatalytic Degradation of p-Toluenesulphonic Acid in Aqueous Systems Containing Powdered and Immobilized Titanium-Dioxide. *Journal of Photochemistry and Photobiology a-Chemistry* **1994**, 83 (1), 69-75.
2. Zhang, H. M.; Quan, X.; Chen, S.; Zhao, H. M.; Zhao, Y. Z., Fabrication of photocatalytic membrane and evaluation its efficiency in removal of organic pollutants from water. *Separation and Purification Technology* 2006, 50 (2), 147-155.
3. Chong, M. N.; Jin, B.; Chow, C. W. K.; Saint, C., Recent developments in photocatalytic water treatment technology: A review. *Water Research* 2010, 44 (10), 2997-3027.
4. Mozia, S., Photocatalytic membrane reactors (PMRs) in water and wastewater treatment. A review. *Separation and Purification Technology* 2010, 73 (2), 71-91.
5. Bosc, F.; Ayril, A.; Guizard, C., Mesoporous anatase coatings for coupling membrane separation and photocatalyzed reactions. *Journal of Membrane Science* 2005, 265 (1-2), 13-19.
6. Bosc, F.; Ayril, A.; Guizard, C., Mesoporous anatase coatings for coupling membrane separation and photocatalyzed reactions. *Journal of Membrane Science* 2005, 265 (1-2), 13-19.
7. Athanasekou, C. P.; Romanos, G. E.; Katsaros, F. K.; Kordatos, K.; Likodimos, V.; Falaras, P., Very efficient composite titania membranes in hybrid ultrafiltration/photocatalysis water treatment processes. *Journal of Membrane Science* 2012, 392, 192-203.
8. Wang, W. Y.; Irawan, A.; Ku, Y., Photocatalytic degradation of Acid Red 4 using a titanium dioxide membrane supported on a porous ceramic tube. *Water Research* 2008, 42 (19), 4725-4732.
9. Kim, Tae-Hyun, and Byeong-Hyeok Sohn. "Photocatalytic Thin Films Containing TiO₂ Nanoparticles by the Layer-by-layer Self-assembling Method." *Applied Surface Science* 201.1-4 (2002): 109-14.
10. Sobczyk-Guzenda, A.; Pietrzyk, B.; Szymanowski, H.; Gazicki-Lipman, M.; Jakubowski, W., Photocatalytic activity of thin TiO₂ films deposited using sol-gel and plasma enhanced chemical vapor deposition methods. *Ceramics International* 2013, 39 (3), 2787-2794.
11. Ding, Z.; Hu, X. J.; Yue, P. L.; Lu, G. Q.; Greenfield, P. F., Synthesis of anatase TiO₂ supported on porous solids by chemical vapor deposition. *Catalysis Today* 2001, 68 (1-3), 173-182.

12. Julbe, Anne, Vincent Rouessac, Jean Durand, and André Ayrál., New Approaches in the Design of Ceramic and Hybrid Membranes. *Journal of Membrane Science* 316.1-2 (2008): 176-85.
13. Rahn, R. O., Potassium iodide as a chemical actinometer for 254 nm radiation: Use of iodate as an electron scavenger (vol. 66, pg. 450, 1997). *Photochemistry and Photobiology* **1997**, 66 (6), 885-885.
14. Guo, B.; Pasco, E. V.; Xagorarakí, I.; Tarabara, V. V. Virus removal and inactivation in a hybrid microfiltration-UV process with a photocatalytic membrane. *Separ. Purif. Technol.* 2015, 149, 245–254.
15. Rahn, R. O.; Xu, P.; Miller, S. L., Dosimetry of room-air germicidal (254 nm) radiation using spherical actinometry. *Photochemistry and Photobiology* **1999**, 70 (3), 314-318.
16. Porter, J. F.; Li, Y. G.; Chan, C. K., The effect of calcination on the microstructural characteristics and photoreactivity of Degussa P-25 TiO₂. *Journal of Materials Science* **1999**, 34 (7), 1523-1531.
17. Priya, D. N.; Modak, J. M.; Raichur, A. M., LbL Fabricated Poly(Styrene Sulfonate)/TiO₂ Multilayer Thin Films for Environmental Applications. *Acs Applied Materials & Interfaces* **2009**, 1 (11), 2684-2693.
18. Zhang, H. M.; Quan, X.; Chen, S.; Zhao, H. M.; Zhao, Y. Z., Fabrication of photocatalytic membrane and evaluation its efficiency in removal of organic pollutants from water. *Separation and Purification Technology* **2006**, 50 (2), 147-155.

CHAPTER 3

Photocatalytic membranes for virus inactivation

3.1 Introduction

Photocatalysis has been proposed as a means of disinfection since 1985, when Matsunga et al successfully inactivated *Lactobacillus acidophilus*, *Saccharomyces cerevisiae*, and *Escherichia coli* in suspended TiO₂/Pt catalyst [1]. This work has since been extended to other microorganisms, including the photocatalytic inactivation of bacteriophages [2] and human viruses [3]. As shown by Cho, viruses pose a more significant challenge for photocatalytic inactivation than bacteria, which the authors attributed to the lack of enzymes and other sensitive systems in viruses [4].

While a majority of photocatalytic disinfection research has focused on using suspended catalytic reactors, thin film technologies have been proposed as a practical means of implementing photocatalytic disinfection [5]. This application eliminates concerns of catalyst aggregation and the need for catalyst recovery systems. Using a membrane as a thin film contactor, the resulting photocatalytic membrane, depending on the catalyst location, has several benefits to the photocatalytic and separative functions; the benefits include reduced fouling, reduced turbidity during photocatalysis, and concentration of pollutants near catalyst surfaces.

As described in Chapter 2, a novel photocatalytic membrane was prepared using LbL self-assembly to apply TiO₂ catalyst to the support structure of a ceramic disc membrane. This study investigates the use of this photocatalytic membrane for inactivation of MS2 and P22 bacteriophages. The inactivation of the bacteriophages using a photocatalyst is a multi-step

process that includes diffusion of the phage through the boundary layer, absorption to the catalyst, inactivation of the phage, and desorption away from the catalyst. In this context, testing the photocatalytic inactivation of MS2, a 20 nm spherical RNA phage and P22, a 60 nm DNA phage with a tail, provides an interesting comparison and can lend insight into the selection and design of photocatalytic processes.

3.2 Experimental

3.2.1 Reagents

The membrane modified by a 5-layer LbL self-assembled coating (see Chapter 2) was used in all photocatalytic filtration experiments. Degussa P25 TiO₂ nanoparticles were used for batch experiments. MS2 was acquired from ATCC (15597-B1) and P22 was acquired from Professor Charles P. Gerba at the University of Arizona.

3.2.2 Batch Experiments

The batch reactor consisted of a UV exposure box, UV lamp (16 W, model GPH330T5L/4, Atlantic Ultraviolet Corp), stir plate, and a beaker (Figure 1b). The UV lamp is within the germicidal range, with 95% of emitted energy at 254 nm. Details on fluence quantification are provided in chapter 2. Batch experiments with P25 were conducted with MS2 and P22 bacteriophages. A 1,000 mg/L catalyst suspension was prepared by suspending P25 in DI water

and adjusting the pH to 5 using HCl. This suspension was sonicated for 30 minutes using a probe sonicator. A prescribed amount of the suspended catalyst was then added to the bacteriophage spiked solutions, resulting in a 1.25 mg/L suspension of catalyst. After the catalyst was added, the solution was stirred and allowed to equilibrate for 10 minutes prior to UV exposure. During the batch test, the fluid remained stirred and samples were taken at periodic intervals.

3.2.3 Dead-end filtration experiments

A UV dead-end filtration test apparatus was constructed by machining a permeate window in a 47 mm diameter stainless steel dead-end filtration cell (Sterlitech). A 1/8" thick quartz glass disc (Technical Glass Products) was fit into the window with a glass hose barb to capture the permeate stream. During UV dead-end filtration experiments, the membrane holder was positioned such that the permeate window was uniformly exposed to UV light. The dead-end filtration experiments utilized the same UV exposure box and UV lamp as the batch reaction experiments. All dead-end filtration experiments were conducted with a constant pressure configuration and permeate samples were collected for 20 minutes prior to UV exposure to account for adsorption of bacteriophages to the membrane, filtration cell, and tubing. Permeate samples were then taken periodically after exposure to UV. Permeate flow rate was recorded with a data acquisition system.

3.2.4 Quantification of bacteriophage concentration

Bacteriophage culturing and quantification was performed by The Water Quality, Environmental, and Molecular Microbiology Laboratory at Michigan State University. Samples were diluted in phosphate buffered water and replicate volumes of the dilution series were analyzed by double agar overlay, using a host bacterium in the logarithmic growth phase to produce plates with countable plaques after 16-24 hour incubation at 37°C. The host bacterium for MS2 was *E.coli* Famp (ATCC # 700891). *E.coli* Famp was grown and maintained in Tryptic Soy Broth (Becton Dickson) with ampicillin and streptomycin to maintain the F+ plasmid. The host bacterium for P22 was *Salmonella* LT2 (pLM2) 1217 (HER #1023). Each replicate plate is an assay of 2ml of the sample, either undiluted or diluted. MS2 and P22 were cultured overnight and then filtered through a 0.22 µm membrane to remove bacterial cells. This filtrate was used as the spiking suspension. The MS2 and P22 suspensions used for the photocatalytic batch and dead-end filtration experiments were created by mixing the spiking suspension with laboratory reagent water (Type 2) that had been sterilized by autoclaving. The pH of the suspension was adjusted to below 5 with HCl. The target concentration of the viral suspensions was 10⁸ plaque forming units (PFU) per ml.

3.3 Results and Discussion

3.3.1 Bacteriophage batch experiments

Photocatalytic inactivation of MS2 and P22 in a batch reactor was performed with Degussa P25 catalyst, Figure 10. The initial MS2 concentration was 2.5×10^8 PFU/mL and the initial P22 solution contained 4.0×10^6 PFU/mL. A 5.5 log removal of MS2 was achieved after 734 mJ/cm^2 fluence exposure. A 2.9 log removal of P22 was achieved after 73.5 mJ/cm^2 UV fluence. Both bacteriophages show a log-linear dependence on exposure time to UV, indicating pseudo-first order kinetics, with MS2 having a reaction constant of 0.011 s^{-1} and P22 having a constant of 0.054 s^{-1} . The reaction constant for MS2 is in line with reported values by Koizumi [2], who demonstrated a reaction constant of 0.012 s^{-1} , but using a higher catalyst loading and slightly higher wattage lamp. Literature data on using Degussa P25 in a batch reactor to inactivate P22 could not be found for comparison.

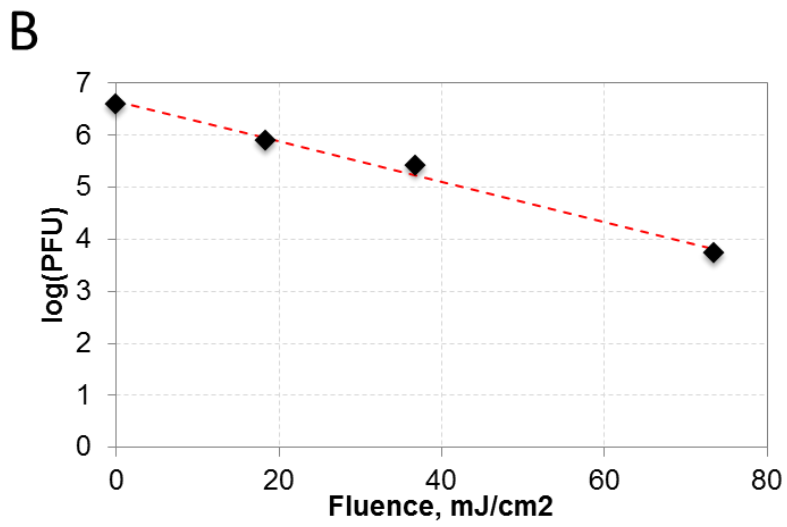
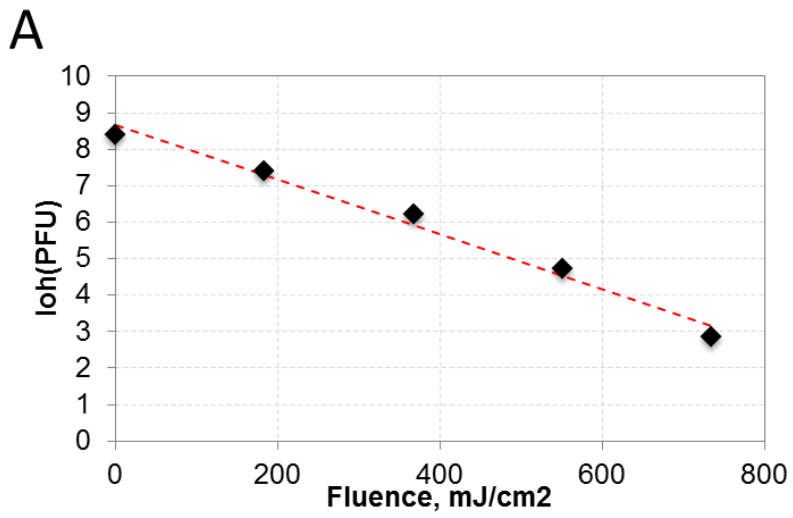
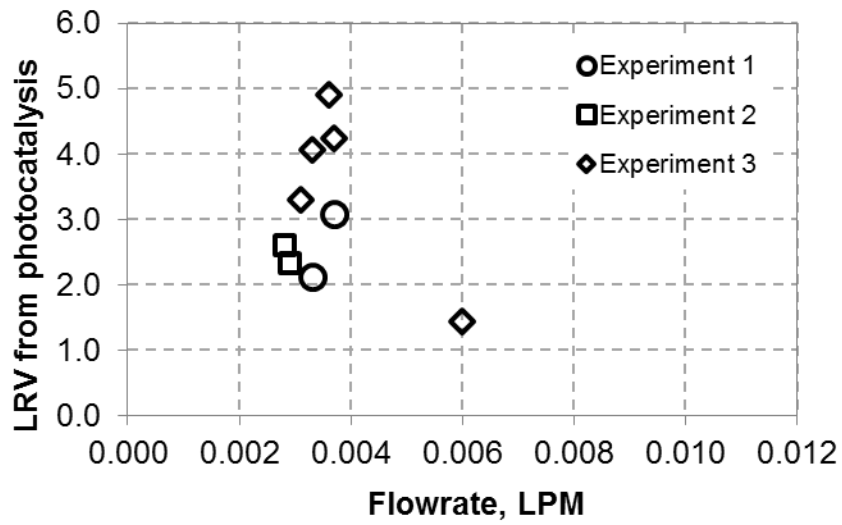


Figure 10: Bacteriophage batch testing using 1.25 mg/L Degussa P25 photocatalyst: A) MS2; B) P22

3.3.2 *UV Bacteriophage dead-end filtration*

Photocatalytic inactivation of MS2 and P22 was investigated with a UV dead-end filtration experiment, Figure 11. Several experiments were performed for each bacteriophage, with each experiment using a new suspension of phages. The Figure plots the log removal value from the photocatalytic activity, not including removal from the membrane. The membrane removed 1.5 LRV of MS2 and 0.7 LRV of P22 prior to UV exposure. As evident from Figure 10A, the MS2 experiments displayed a wide range of LRV. For example, at 3.3×10^{-3} liters per minute, the log removal value varied between experiments from 2.1 to 4.1. Similarly for P22, at 9.0×10^{-3} liters per minute the log removal varied from 1.8 to 1.1. With a limited data set and high variability, statistical inference is difficult. Qualitatively, MS2 appears to have a generally higher rate of removal than P22. This is an interesting result since P22 had higher kinetics in batch experiments.

A



B

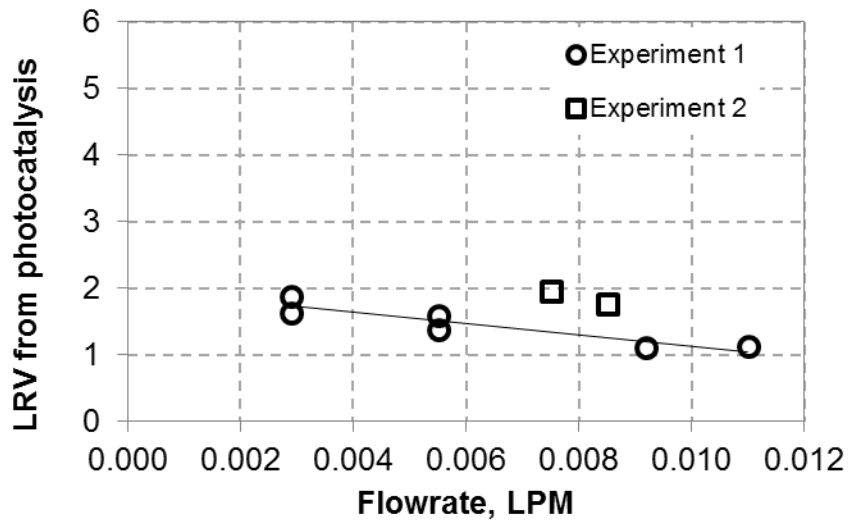


Figure 11: UV dead-end filtration experiments A) MS2 B) P22

3.4 Conclusion

The inactivation of MS2 and P22 was tested using a batch reactor with suspended Degussa P25 photocatalyst and a UV dead-end filtration process using a photocatalytic membrane. During batch testing both phages displayed first order kinetics. A 0.3 log removal of MS2 was achieved with 73.5 mJ/cm² fluence compared to 2.9 log removal of P22 at the same fluence dose. With UV dead-end filtration, significant variation occurred between experiments and made a quantitative conclusion difficult, though in contrast to batch experiments, during UV dead-end filtration, MS2 appears to be more susceptible to inactivation than P22. This contrast may be attributed to differences in the physical properties of P22 and MS2. P22, due to its larger size, has a smaller diffusion coefficient, resulting in a lower concentration of available phages at the catalyst surface. Additionally, the larger size of P22 may result in more damage to the phage as it permeates the membrane. Differences in the surface properties may have affected the adsorption-desorption rate of each phage on the catalyst surface, resulting in different inactivation kinetics. Also bacteriophage aggregation, such as caused by a change in pH during batch experiments, may have reduced the apparent viable phage count. Lastly, the contrasting results may be attributed to experimental error, such as not reaching the dead-end test apparatus absorption capacity for P22 prior to UV exposure. This study resulted in an interesting comparison on the suitability of UV dead-end filtration and batch processes for bacteriophage inactivation. Further investigation to determine the cause of the contrasting results will provide useful knowledge in the selection and design of photocatalytic processes for virus inactivation.

REFERENCES

REFERENCES

1. Matsunaga, T.; Tomoda, R.; Nakajima, T.; Wake, H., Photoelectrochemical sterilization of microbial-cells by semiconductor powders. *Fems Microbiology Letters* 1985, 29 (1-2), 211-214.
2. Koizumi, Y.; Taya, M., Kinetic evaluation of biocidal activity of titanium dioxide against phage MS2 considering interaction between the phage and photocatalyst particles. *Biochemical Engineering Journal* 2002, 12 (2), 107-116.
3. Nakano, R.; Ishiguro, H.; Yao, Y. Y.; Kajioka, J.; Fujishima, A.; Sunada, K.; Minoshima, M.; Hashimoto, K.; Kubota, Y., Photocatalytic inactivation of influenza virus by titanium dioxide thin film. *Photochemical & Photobiological Sciences* 2012, 11 (8), 1293-1298.
4. Cho, M.; Chung, H. M.; Choi, W. Y.; Yoon, J. Y., Different inactivation Behaviors of MS-2 phage and *Escherichia coli* in TiO₂ photocatalytic disinfection. *Applied and Environmental Microbiology* 2005, 71 (1), 270-275.
5. Hajkova, P.; Spatenka, P.; Horsky, J.; Horska, I.; Kolouch, A., Photocatalytic Effect of TiO₂ Films on Viruses and Bacteria. *Plasma Processes and Polymers* 2007, 4, S397-S401.